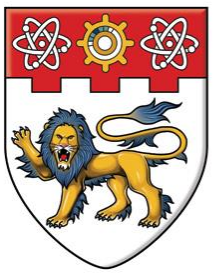

NANYANG TECHNOLOGICAL UNIVERSITY

MODEL BASED MAXIMUM POWER POINT TRACKING FOR SATELLITE APPLICATION

LEW JIA MIN

SCHOOL OF ELECTRICAL & ELECTRONIC ENGINEERING

2017

Model Based Maximum Power Point Tracking for Satellite Application

LEW JIA MIN

LEW JIA MIN

School of Electrical & Electronic Engineering

A thesis submitted to the Nanyang Technological University

in fulfilment of the requirement for the degree of

Master of Engineering

2017

ACKNOWLEDGEMENT

It has been a long journey to complete my Master of Engineering studies. I would like to express my heart-felt thanks to everyone who have been there to support me throughout the journey.

First and foremost, I would like to express my special appreciation and thanks to my supervisor Professor Low Kay Soon for encouragement and guidance during my research. His support throughout my Master of Engineering studies allow me to grow as a better person in life. It is my honour to continue my graduate studies under his supervising. Besides Professor Low, I am also thankful to Associate Professor Ali Iftekhar Maswood for being my supervisor and his assistance during my thesis submission.

Secondly, I would like to thanks my fellow colleagues, Dr. Soon and Dr. Aung for their advice. Their knowledges and experiences in the field of satellite's power supply system (PSS) are valuable to my studies.

Next, I am very thankful to everyone from Satellite Research Centre for providing me an enjoyable working environment. It is my pleasure to work together with my fellow colleagues during my studies.

Finally yet importantly, I would like to give thanks to my family who always support in every decision I made in my life. Without their love and care, I would not have gotten to where I am today. I hope I have made them proud and I dedicate this thesis to my family.

TABLE OF CONTENTS

ACKNOWLEDGEMENT ..... **I**

TABLE OF CONTENTS ..... **II**

LIST OF TABLES ..... **IV**

LIST OF FIGURES ..... **V**

LIST OF ABBREVIATIONS ..... **IX**

ABSTRACT ..... **X**

CHAPTER 1. INTRODUCTION **1**

1.1. Background 1

1.2. Objectives of the Research 3

1.3. Contributions of the Thesis 4

1.4. Outline of Thesis 5

CHAPTER 2. PHOTOVOLTAIC ARRAY MODELLING AND MAXIMUM POWER POINT TRACKING **6**

2.1. Photovoltaic Array Modelling 6

2.2. Maximum Power Point Tracking Methods 10

2.3. Summary 14

CHAPTER 3. CONVENTIONAL MPPT METHODS FOR SATELLITE APPLICATION **16**

3.1. Simulation and Scenarios 16

3.2. Analysis and Evaluation of Simulation Study 21

3.2.1. Normal operating mode 21

3.2.2. Safe-hold operating mode....25

3.3. Summary....29

CHAPTER 4. SOLAR INSOLATION AND MAXIMUM POWER POINT ESTIMATION (SIMPPE)....30

4.1. SIMPPE Algorithm....32

4.2. Feasibility Studies of SIMPPE Algorithm....35

4.3. Simulation Study of SIMPPE Algorithm....50

4.4. Experimental Validation of SIMPPE Algorithm....55

4.5. Summary....58

CHAPTER 5. TEMPERATURE AND MAXIMUM POWER POINT ESTIMATION (TMPPE)....60

5.1. TMPPE Algorithm....61

5.2. Feasibility Studies of TMPPE Algorithm....63

5.3. Simulation Study of TMPPE Algorithm....72

5.4. Experimental Validation of TMPPE Algorithm....77

5.5. Summary....79

CHAPTER 6. CONCLUSION AND FUTURE WORKS....80

6.1. Conclusion....80

6.2. Future Works....82

LIST OF PUBLICATIONS....83

BIBLIOGRAPHY....85

LIST OF TABLES

Table 2.1 Comparison of MPPT methods.....14

Table 3.1 Parameters of components used in PV system 17

Table 3.2 Tracking efficiency under satellite scenario with P&O and InC for different ΔD 28

Table 4.1 PV parameters for simulation study (Azur Space TJ Solar Cell 3G30C).....36

Table 4.2 Summary of solar insolation estimation and MPP estimation.....39

Table 4.3 ADC specification for microcontroller C8051F12x-13x (P/N: C8051F12x-13x) 46

Table 4.4 Solar insolation level estimation error under different satellite operating scenarios.....52

Table 4.5 Comparison of tracking efficiency under different satellite operation scenarios.....54

Table 4.6 Tracking efficiency comparison for the SIMPPE algorithm 58

Table 5.1 Summary of estimation error at 3-sigma (T = 28°C, G = 1353W/m^2) 68

Table 5.2 Comparison of mean absolute error under different satellite operating scenarios.....76

Table 5.3 Comparison of tracking efficiencies under different satellite operating scenarios.....76

Table 5.4 Tracking efficiency comparison for the TMPPE algorithm 78

LIST OF FIGURES

Fig. 2.1 Single diode PV model 6

Fig. 2.2 *I-V* and *P-V* characteristics (at 25 °C and 1000 W/m^2) of a PV cell 8

Fig. 2.3 *I-V* (left) and *P-V* (right) curves under different solar insolation 9

Fig. 2.4 *I-V* (left) and *P-V* (right) curves under different temperature 9

Fig. 2.5 Maximum power point tracking using fuzzy logic control [15] 13

Fig. 3.1 Block diagram of system used to evaluate MPPT methods 17

Fig. 3.2 PSIM simulation model of PV system with conventional MPPT 18

Fig. 3.3 Temperature and solar insolation level profile for satellite under different scenarios (a) normal operating mode with sun-tracking (b) safe-hold operating mode with 2 degrees/s rotation (c) safe-hold operating mode with 4 degree/s rotation (d) safe-hold operating mode with 6 degree/s rotation 19

Fig. 3.4 Rate of change of temperature and solar insolation level for satellite under different scenarios (a) normal operating mode with sun-tracking (b) safe-hold operating mode with 2 degrees/s rotation (c) safe-hold operating mode with 4 degree/s rotation (d) safe-hold operating mode with 6 degree/s rotation 20

Fig. 3.5 Simulated PV output power during the normal operating mode with conventional MPPT algorithm with 1% perturbation size (ΔD) (a) P&O (b) InC 22

Fig. 3.6 Tracking efficiency of P&O and InC during the normal operating mode 23

Fig. 3.7 PV operating point oscillation at steady state with P&O (left) and InC (right) with ΔD (a) 1% (b) 2% (c) 3% (d) 4% (e) 5% during the normal operating mode 24

Fig. 3.8 Tracking power loss at steady-state oscillation, P&O (left) and InC (right) with ΔD (a) 1% (b) 2% (c) 3% (d) 4% (e) 5% under normal operation scenario 25

Fig. 3.9 Simulated PV output power under safe-hold operation scenarios with tracking MPPT algorithm with 1% perturbation size (ΔD) 26

Fig. 3.10 Tracking efficiency of P&O and InC under safe-hold operation scenarios ... 27

Fig. 4.1 PV *I-V* curve (left) and error of solar insolation level estimation (right) under different temperatures and solar insolation level conditions 37

Fig. 4.2 Error of V_{mp} estimation and solar insolation level estimation under different temperature and solar insolation level conditions.....38

Fig. 4.3 Solar insolation level estimation error under different voltage and temperature 41

Fig. 4.4 Maximum solar insolation level estimation error under different temperature and solar insolation level 42

Fig. 4.5 Mean solar insolation level estimation error under different temperature and solar insolation level 42

Fig. 4.6 Maximum V_{mp} estimation error under different temperature and solar insolation level.....44

Fig. 4.7 Mean V_{mp} estimation error under different temperature and solar insolation level.....44

Fig. 4.8 Worst case of tracking efficiency under different temperature and solar insolation level.....45

Fig. 4.9 Comparison of maximum solar insolation level estimation absolute error between ideal scenario and non-ideal scenario (left: 10-bit ADC, right: 12-bit ADC) 47

Fig. 4.10 Comparison of mean solar insolation level estimation absolute error between ideal scenario and non-ideal scenario (left: 10-bit ADC, right: 12-bit ADC) 47

Fig. 4.11 Comparison of maximum V_{mp} estimation absolute error between non-ideal and ideal scenario at nominal temperature (left: full view; right: closer view, G < 200 W/m^2).....48

Fig. 4.12 Comparison of mean V_{mp} estimation absolute error between non-ideal and ideal scenario at nominal temperature (left: full view; right: closer view, G < 200 W/m^2).....48

Fig. 4.13 Comparison of worst case tracking efficiency between non-ideal and ideal scenario at nominal temperature (left: full view; right: closer view, G < 100W/m^2) ...49

Fig. 4.14 PSIM-based simulation model of PV system with the SIMPPE algorithm ..50

Fig. 4.15 Solar insolation estimation absolute error (left) and relative error (right) under different scenarios.....52

Fig. 4.16 V_{mp} estimation absolute error (left) and relative error (right) under different scenarios.....54

Fig. 4.17 Hardware-in-the-loop experimental test setup 56

Fig. 4.18 Experimental tracked power vs simulation tracked power for SIMPPE algorithms under different scenarios.....57

Fig. 5.1 Points used by the TMPPE algorithm.....61

Fig. 5.2 Temperature estimation under different temperature and solar insolation level 64

Fig. 5.3 Absolute mean error of temperature estimation under different measurement noise levels.....65

Fig. 5.4 Absolute mean error of solar insolation level estimation under different measurement noise levels 66

Fig. 5.5 Mean MPP voltage estimation error under different measurement noise levels 67

Fig. 5.6 Mean power loss under different measurement noise levels.....67

Fig. 5.7 Temperature estimation performance under different environmental conditions 69

Fig. 5.8 Solar insolation level estimation performance under different environmental conditions.....69

Fig. 5.9 V_{mp} estimation performance under different environmental conditions.....70

Fig. 5.10 Power loss under different environmental conditions 71

Fig. 5.11 PSIM-based simulation model of PV system with the TMPPE algorithm....72

Fig. 5.12 Temperature and solar insolation level estimation absolute error under different scenarios 74

Fig. 5.13 MPP voltage estimation absolute error under different scenarios 75

Fig. 5.14 Experimental tracked power vs simulation tracked power for TMPPE algorithms under different scenarios 78

LIST OF ABBREVIATIONS

ADC	Analog to digital converter
ADCS	Attitude determination and control system
ANN	Artificial neural network
DC	Direct current
DET	Direct energy transfer
FLC	Fuzzy logic control
FOCV	Fractional open circuit voltage
FSCI	Fractional short circuit current
GPIB	General purpose interface bus
InC	Incremental conductance
LEO	Low earth orbit
MOSFET	Metal-oxide-semiconductor field-effect-transistor
MPP	Maximum power point
MPPT	Maximum power point tracking
OBDH	On board data handling
P&O	Perturb and observe
PSIM	Powersim
PSO	Particle swarm optimization
PSS	Power supply system
PV	Photovoltaic
SIMPPE	Solar insolation and MPP estimation
TLE	Two line element
TMPPE	Temperature and MPP estimation

ABSTRACT

For a satellite, the primary power source is the solar energy. The amount of harvested solar energy will determine the depth of discharge of the battery in each orbit. This will in term decides the lifespan of the satellite. Hence, the ability to extract the maximum power from the Sun given any operating condition is important.

In this thesis, perturb and observe (P&O) and incremental conductance (InC) maximum power point tracking (MPPT) methods have been studied for nano-satellites applications. There are two main operating scenarios of a satellite in space, namely the normal operation mode and safe-hold operation mode. The former is when the satellite is stabilized with its photovoltaic (PV) array pointing to the Sun. The latter is when the satellite experiences rotation and each PV array will face the Sun for a short period.

From the simulation study, it is observed that the P&O and InC have inconsistent tracking performance with a reduced efficiency when the satellite is rotating. On the other hand, they have similar performance with efficiency up to 99% for normal operating scenario where the PV of satellite is facing towards the Sun.

To overcome the shortcoming of poor tracking efficiency when the satellite is rotating, a new model based MPPT algorithm with solar insolation and maximum power point estimation (SIMPPE) concept is proposed. The SIMPPE algorithm uses voltage, current and temperature measurements incorporated into a single diode PV model to estimate the PV solar insolation level. This is then used to reconstruct the *I*-*V* curve and the estimate of maximum power point (MPP) voltage of the PV array. The simulation results show that the SIMPPE algorithm has a tracking efficiency of above 97% for all satellite operating scenarios. The hardware-in-the-loop test system with

solar array simulators and electronic loads is used for experimental validation. In the experimental studies, the results show that the tracking efficiency for the SIMPPE algorithm has consistent tracking efficiency of 91% when the satellite is rotating.

A temperature and MPP estimation (TMPPE) algorithm has been proposed to improve the SIMPPE algorithm by eliminating the PV temperature measurement to reduce number of sensor. The TMPPE algorithm uses four pairs of voltage and current measurements incorporated into a single diode PV model to estimate PV temperature and solar insolation simultaneously. The identified PV environmental conditions will then be used to reconstruct *I-V* curve and estimate MPP voltage. The simulation result shows that the TMPPE algorithm has improved tracking efficiency compared to conventional MPPT methods when the satellite is rotating. The TMPPE algorithm has been validated experimentally using hardware-in-the-loop test system. The experimental results show that the tracking efficiency for the TMPPE algorithm under normal operating and safe-hold operating scenarios are 94% and 87% respectively.

CHAPTER 1. **INTRODUCTION**

1.1. **Background**

Miniaturized satellites such as nanosatellites and pico-satellites have become an attractive platform for educational institutions and commercial companies to carry out space science research and applications [1-5]. The main reason is its reduced cost and shorter development time as compared to larger satellites. With the advancement in technologies, the size and mass of satellite components have been greatly reduced [1]. This allows the miniaturized satellites to incorporate more advanced payloads with space and mass constraints.

A satellite consists of many subsystems such as power supply system (PSS), attitude control and determination system (ADCS), on board data handling (OBDH) system, communication system and payloads. Among the many subsystems, PSS is one of the key systems for any satellite [6, 7]. The role of PSS is to generate, store, regulate and distribute electrical power to other subsystems. There are several possible power sources for satellites, which are nuclear, photovoltaic (PV), and chemical [8]. Nuclear power has large power density gives the advantage of limitless energy and is more suitable for deep space application [9, 10]. For earth-orbiting satellites, in particular low-earth-orbit (LEO) satellites, nuclear power is not suitable due to environmental issue. During the atmospheric entry, the satellite will re-enter to the Earth and cause radioactive particles spread over the Earth's atmosphere [8]. For chemical power source, the fuel mass limits its lifetime. As the satellite mission time increases, the satellite mass will be totally dominated by the fuel mass alone. Thus,

chemical power source such as fuel cells and rechargeable batteries are always used in conjunction with solar panels for LEO satellites.

The PSS uses PV arrays, usually in the form of one or several solar panels, carrying a number of PV cells to convert sunlight into electricity. The behaviour of each PV array can be represented by a non-linear current-voltage (*I-V*) characteristic. In every PV array, there is a unique operating point known as the maximum power point (MPP) that is the optimal point to operate the PV array and produce maximum power output. There are two factors, namely the cell temperature and the insolation level, that vary the MPP [11]. Therefore, any variation in either one of these factors change the location of the PV array's MPP. Thus, it is necessary to constantly monitor and adjust the PV array operating point accordingly to extract optimal power at a given environmental condition.

The MPP of PV arrays can be tracked using maximum power point tracking (MPPT) methods. Many MPPT methods [12-34] have been reported and they can be classified into conventional and artificial intelligent methods. The conventional methods include perturb and observe (P&O) algorithm [16-23], incremental conductance (InC) algorithm [24-28], fractional open circuit voltage (FOCV) [29-31], and fractional short circuit current (FSCI) [29, 32]. For the artificial intelligent method, it includes fuzzy logic control (FLC) [33, 34] and artificial neural network (ANN). The conventional MPPT methods are widely applied due to their simplicity and ease of implementation. Most of the conventional MPPT methods exhibit high performance under stable environment conditions only. On the other hand, the artificial intelligent MPPT methods are more complex but they are more efficient and response faster.

For miniaturized satellites application, P&O method is widely used due to its simplicity and low computational cost [35-37]. For satellites without any stabilization control, the PV arrays will encounter rapid changes in temperature and solar insolation due to the rotation of the satellite. Therefore, conventional MPPT methods such as P&O and InC that are used in steady-state condition might not be suitable for such application. Other than P&O and InC methods, FOCV and FSCI are not recommended for miniaturized satellite application because they operate the PV under open circuit or short circuit condition, which may interrupt the operation of the satellite.

To overcome the environmental issues and better optimize the power from the PV array, the aim of this thesis is to investigate and propose a suitable MPPT method for satellite application. This will enable the satellite to harvest its maximum power under varying conditions, which helps prolong satellite's operating lifespan.

1.2. **Objectives of the Research**

The aims of this research are as follows:

- The environmental condition for PV array in satellite application is different compared to ground based PV application. Therefore, the first objective of this thesis will be to study the performance of conventional MPPT methods for satellite application.
- Based on the simulation study, the performance of conventional MPPT methods is investigated. Thus, the next objective is to propose a new MPPT method, which exhibits no steady-state oscillation and perform better than conventional MPPT methods under varying environmental conditions in space.

- The performance of the proposed MPPT method will be analyzed based on software-based simulations. Therefore, the last objective of this thesis is to validate the new proposed MPPT method experimentally using hardware-in-the-loop test system.

1.3. **Contributions of the Thesis**

- A simulation study of conventional MPPT of P&O and InC for satellite application has been conducted. In the study, the performance of P&O and InC under different satellite operation scenarios have been evaluated.

- A new algorithm, solar insolation and MPP estimation (SIMPPE) algorithm is proposed. The SIMPPE algorithm does not require special sensor such as pyranometer. Instead, the solar insolation is estimated with the voltage, current and temperature measurements. With the estimated solar insolation, the MPP voltage of the PV can be determined using numerical method.

- A new algorithm, temperature and MPP estimation (TMPPE) is proposed to improve the SIMPPE algorithm by eliminating temperature measurement. With four pairs of voltage and current measurements near MPP, the temperature and solar insolation can be estimated. With the estimated environmental parameters, the MPP voltage can be estimated by solving PV *I*-*V* equation using numerical method.

1.4. **Outline of Thesis**

This thesis is organized as follows:

Chapter 2 presents a review on photovoltaic (PV) array modelling and MPPT techniques. The PV model and its characteristics under different temperatures and solar insolation are discussed in details. The conventional and artificial intelligent MPPT techniques and their limitations will be explained.

Chapter 3 presents a simulation study of conventional MPPT techniques for satellite's application. A Powersim (PSIM) based simulation has been conducted for satellite operation scenarios to analyze the performance of P&O and InC.

Chapter 4 presents the proposed MPPT technique to address the problems determined in Chapter 3. The performance of the proposed method has been analyzed in various temperatures and solar insolation scenarios. Simulation study has been conducted for satellite scenario to analyze the performance of proposed method and the results are compared with the conventional MPPT methods.

Chapter 5 presents an improvement on proposed MPPT technique in Chapter 4. The improved model based MPPT method is able to estimate PV temperature and solar insolation at the same time. This chapter also analyzed the measurement noise effect on the performance of the proposed method. The performance of the improved method has been evaluated with simulation study for satellite scenario.

Chapter 6 concludes the thesis and presents the future works.

CHAPTER 2. PHOTOVOLTAIC ARRAY MODELLING AND MAXIMUM POWER POINT TRACKING

This chapter models the output characteristic of the single diode model and its changes to temperature and solar insolation level is discussed. The advantages and disadvantages of conventional maximum power point tracking (MPPT) methods are also reviewed.

2.1. Photovoltaic Array Modelling

A PV array in the PSS of a satellite is used to convert sunlight into electrical energy. It is formed by connecting a number of PV cells in series-parallel combination to achieve the required system voltage and current.

Fig. 2.1 shows a single diode PV model of a PV cell. The single diode model is widely used due to its simplicity with acceptable accuracy [38-42]. It consists of a current source, a diode, a series and a parallel resistor. The series resistor represents the ohmic loss and the parallel resistor represents the leakage of the PV cell.

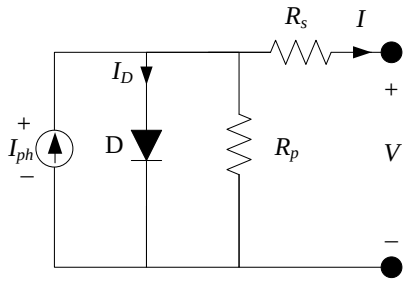

Fig. 2.1 Single diode PV model

Applying Kirchhoff's current law to Fig. 2.1, the external load current I can be written as:

$$I = I_{ph} - I_D - \frac{V + R_s I}{R_p} \tag{2.1}$$

where

I_{ph} : generated photo current

I_D : diode current

V : external load voltage

The diode current, I_D is represented by the schlocky equation which is given by:

$$I_D = I_{rs}\left[\exp\left(\frac{V + R_s I}{aN_s V_t}\right) - 1\right] \tag{2.2}$$

where

I_{rs} : cell reverse saturation current

a : the diode ideality factor

N_s : number of PV cells connected in series

V_t : thermal voltage, (kT/q), k is Boltzmann's constant ($1.3806503 \times 10^{-23}$ J/K),

T is the junction temperature, q is electron charge ($1.60217646 \times 10^{-19}$ C)

By substituting (2.2) into (2.1), the PV cell *I*-*V* characteristic can be expressed as:

$$I = I_{ph} - I_{rs}\left[\exp\left(\frac{V + R_s I}{aN_s V_t}\right) - 1\right] - \frac{V + R_s I}{R_p} \tag{2.3}$$

For a given temperature and insolation level, the electrical characteristic of the PV cell can be represented by current-voltage (*I*-*V*) curve and power-voltage (*P*-*V*) curve. In Fig. 2.2, the top figure shows the *I*-*V* curve while the bottom figure shows the *P*-*V* curve. In the *I*-*V* and *P*-*V* curves, there are four important parameters that are used to describe the PV cell characteristics. They are the open circuit voltage (V_{oc}), the short

circuit current (I_{sc}), the maximum power point voltage (V_{mp}) and the maximum power point current (I_{mp}).

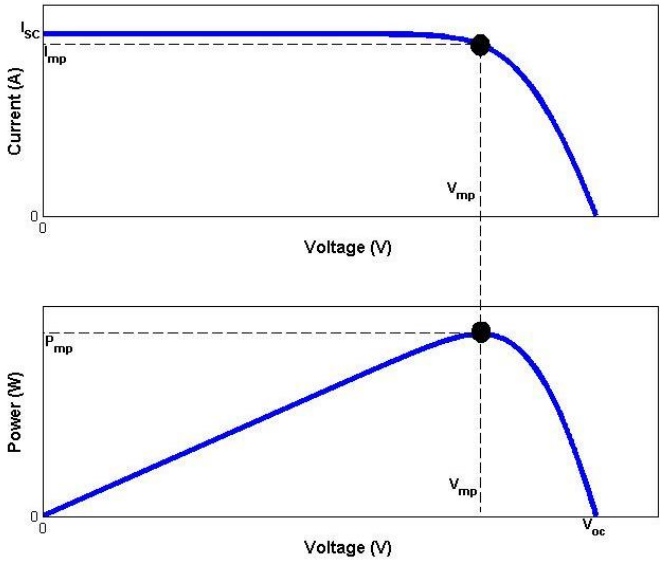

Fig. 2.2 *I-V* and *P-V* characteristics (at 25 °C and 1000 W/m^2) of a PV cell

By substituting $I = I_{sc}$ and $V = 0$ into (2.3), the short circuit current, I_{sc} can be expressed as:

$$I_{sc} = \left(\frac{R_p}{R_p + R_s}\right)\left\{I_{ph} - I_{rs}\left[\exp\left(\frac{R_s I_{sc}}{aN_s V_t}\right) - 1\right]\right\} \tag{2.4}$$

Under the short circuit condition, the diode current are negligible so the short-circuit current is equivalent to the generated photocurrent, I_{ph} which is proportional to the solar insolation level.

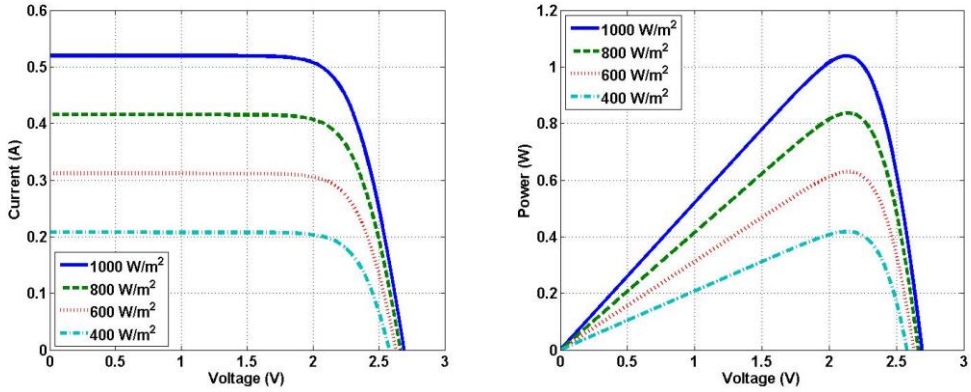

Fig. 2.3 *I-V* (left) and *P-V* (right) curves under different solar insolation

Fig. 2.3 shows the generated *I-V* and *P-V* curves under different insolation levels. From Fig. 2.3, it can be observed that the short circuit current will be reduced significantly when the solar insolation is reduced. Moreover, the maximum power P_{mp} is also reduced as the solar insolation level is reduced.

When the PV cell is at $I = 0$ and $V = V_{oc}$, (2.3) becomes:

$$V_{oc} = R_p \left\{ I_{ph} - I_{rs} \left[\exp\left(\frac{qV_{oc}}{kTa} \right) - 1 \right] \right\} \tag{2.5}$$

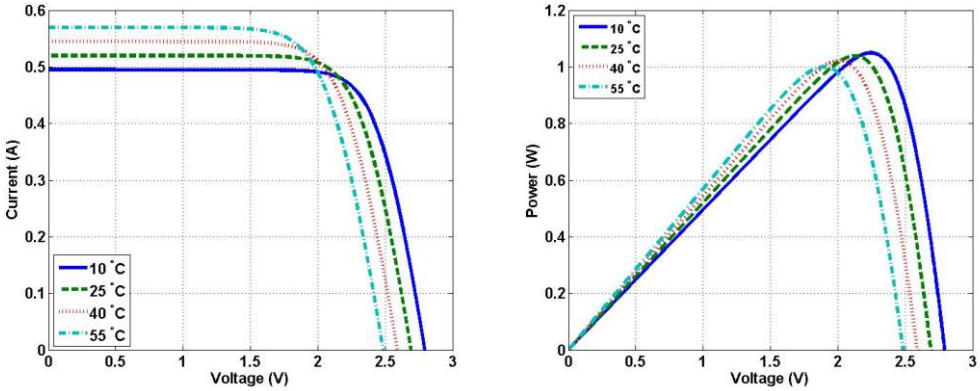

Fig. 2.4 *I-V* (left) and *P-V* (right) curves under different temperature

Fig. 2.4 shows the generated *I-V* and *P-V* curves under different temperature. Under open circuit condition, the open circuit voltage is proportional to the

temperature as shown in (2.5). For variation of temperature in Fig. 2.4, it is observed that open circuit voltage decreases as the temperature increases from 10 °C to 55 °C.

2.2. **Maximum Power Point Tracking Methods**

A PV array is used in the PSS to harvest solar energy and charging of the batteries [43]. There are two general topologies available for satellite electrical power subsystem, which are the direct energy transfer (DET) and maximum power point tracking (MPPT). For DET approach, it operates the PV arrays at a fixed point to transfer power from PV array to the satellite main bus. It is simple to implement and practical if the satellite is experiencing small variation in illumination and long sunlight period. The drawback of DET approach is its poor efficiency if the maximum power point (MPP) of PV array is varying during sunlight period [35]. This is the case for satellite that operates in low earth orbit (LEO). Therefore, a MPPT topology is preferred in particular for miniacturized satellite that is under varying temperatures and solar insolation level.

Many conventional and intelligent MPPT methods have been presented in literature for ground-based PV applications. The most common method is the perturb and observe (P&O) method [16-23]. This method uses the PV array power characteristic to track MPP. The PV array power curve can be expressed in the following equations:

$$\frac{dP}{dV} = 0, \text{ at the MPP } (V_{PV} = V_{mp}) \tag{2.6}$$

$$\frac{dP}{dV} > 0, \text{ at left side of the MPP } (V_{PV} < V_{mp}) \tag{2.7}$$

$$\frac{dP}{dV} < 0 \text{, at right side of the MPP } (V_{PV} > V_{mp}) \tag{2.8}$$

P&O method uses voltage perturbation to determine the direction of tracking using (2.6)-(2.8). Current perturbation is less preferred due to its slow response under changes in solar insolation level and sensitivity to noise [16]. The method operates by periodically perturbing the PV arrays output voltage and compares the output power of the PV arrays in the current perturbation cycle with the previous cycle. If the PV arrays output power increases, then the perturbation of PV arrays output voltage is in the correct direction, otherwise it should be reversed. The major drawbacks of this method are oscillation at MPP during steady state and poor performance under rapidly environmental changes such as solar insolation level. To reduce the oscillation at MPP, variable step-size P&O methods [17-19] have been proposed to increase power drawn from PV arrays.

The other commonly used algorithm is the incremental conductance (InC) method [24-28]. This method works on similar principle as the P&O method [44]. The derivative of power with respect to the voltage ($\frac{dP}{dV}$) can be written in terms of arrays current and voltage:

$$\frac{dP}{dV} = \frac{d(IV)}{dV} = I + V\left(\frac{dI}{dV}\right) \tag{2.9}$$

With (2.9), the PV array power curve can be rewritten in following equations:

$$\frac{dI}{dV} = -\frac{I}{V} \text{ , at the MPP} \tag{2.10}$$

$$\frac{dI}{dV} > -\frac{I}{V} \text{ , at left side of the MPP} \tag{2.11}$$

$$\frac{dI}{dV} < -\frac{I}{V} \text{ , at right side of the MPP} \tag{2.12}$$

Hence, InC method can track the MPP by comparing instantaneous conductance ($\frac{I}{V}$) to the incremental conductance ($\frac{dI}{dV}$). It has a better performance than P&O in both fast changing environment and stable environment. Similar to P&O method, it has the drawback of oscillation at MPP. Some improvements have been made to InC method such as variable perturbation size InC method [26] and power-increment-aided InC [27].

Other than P&O and InC, there are other simple approaches to estimate MPP based on some measurement. Fractional open circuit voltage (FOCV) [29-31] and fractional short circuit current (FSCI) [32] are single-sensor approaches that make use of open circuit voltage or short circuit current of the PV array to estimate the MPP via a near linear equation which are expressed as:

$$V_{mp} \approx k_1 V_{oc} \tag{2.13}$$

$$I_{mp} \approx k_2 I_{sc} \tag{2.14}$$

where

V_{mp}: maximum power point voltage

k_1: voltage constants of proportionality

V_{oc}: open circuit voltage

I_{mp}: maximum power point current

k_1: current constants of proportionality

I_{sc}: short circuit current

In (2.13)-(2.14), the constants of proportionality k_1 and k_2 depend on the PV array characteristic. They can be computed beforehand by analysing the PV arrays at varying solar insolation and temperatures. The disadvantage of these two methods is the requirement to operate the PV arrays at open circuit or short circuit condition to measure V_{oc} or I_{sc} which will cause temporary loss of power. Since these two methods are only estimation technique, the PV arrays is not operating at MPP.

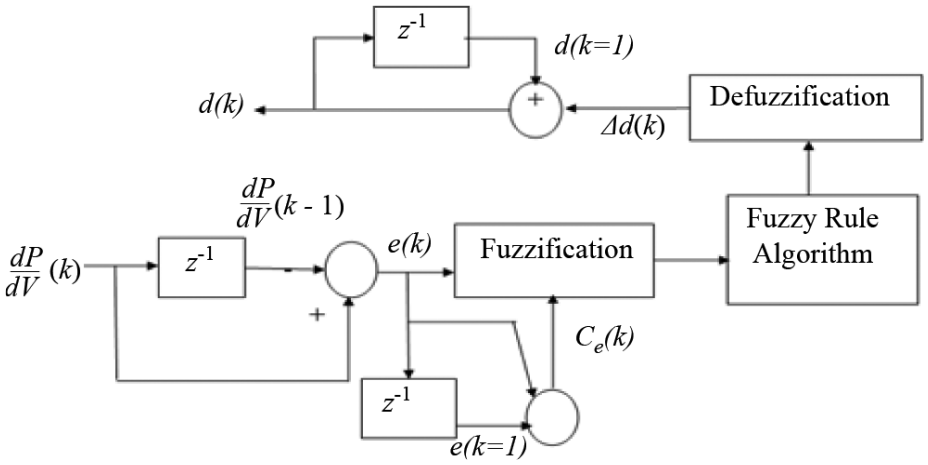

Fig. 2.5 Maximum power point tracking using fuzzy logic control [15]

A fuzzy logic control (FLC) is one of the intelligent techniques proposed to solve MPPT problem [33, 34]. Fig. 2.5 shows one of the FLC solutions for MPPT. There are three stages in this technique, namely fuzzification, inference and defuzzification. During the fuzzification stage, the inputs of the FLC are the error E (i.e. change of $\frac{dP}{dV}$

as shown in Fig. 2.5) and a change in error ΔE. The inference stage will express these two input variables in terms of linguistic variables and the FLC output will be looked up in a given rule-based table. The output of FLC will then be converted from linguistic form to value in defuzzification stage. FLC has the advantages of fast response with no overshoot and less fluctuation in steady state for rapidly changing environment. However, the effectiveness of FLC depends on the formulation of error E and rule-based table.

2.3. **Summary**

This chapter presented a review of photovoltaic array modelling and commonly used MPPT methods. It was identified that the PV array has non-linear output characteristic that is dependent on temperature and solar insolation level. Therefore, maximum power point tracking method is required to exploit the full potential of the PV array. A summary of maximum power point tracking methods discussed in this chapter is shown in Table 2.1.

Table 2.1 Comparison of MPPT methods

MPPT method	Advantages	Disadvantages
P&O	Simplicity, good performance under stable environment	Trade-off between steady-state oscillations and tracking speed, poor performance under rapidly changing irradiance environment
InC	Good performance under rapidly changing environment	Trade-off between steady-state oscillations and tracking speed
FOCV	Require only one voltage sensor, no steady-state oscillation	Required periodic tuning, not true MPP
FSCI	Require only one current sensor, no steady-state oscillation	Required periodic tuning, not true MPP
FLC	Fast response with no overshoot	High complexity

As the space environment differs from the ground environment, there is a need to investigate the performance of conventional MPPT methods for space application. A simulation study of conventional MPPT methods will be presented in Chapter 3. A new model based MPPT method with solar insolation estimation will be proposed in Chapter 4.

CHAPTER 3. CONVENTIONAL MPPT METHODS FOR SATELLITE APPLICATION

The amount of harvested energy for an orbiting satellite depends on the performance of maximum power point tracking (MPPT). In this chapter, the performance of conventional MPPT methods for space applications will be presented. Among the conventional MPPT methods presented in Chapter 2, perturb and observe (P&O) and incremental conductance (InC) have been selected for the study as they have been extensively used in many industrial application. The study is conducted using a Powersim (PSIM) based simulation to evaluate the performance of P&O and InC MPPT methods for space applications. The simulation study has been conducted for two different satellite scenarios, namely the normal operation and the safe-hold operation. A boost converter topology that is used in VELOX-I nano-satellite will be used in this simulation study.

3.1. **Simulation and Scenarios**

Fig. 3.1 shows the block diagram of the system used to study the MPPT methods. It consists of a PV array, a DC/DC boost converter, and a battery. Two conventional MPPT algorithms namely the P&O and InC methods have been implemented for the MPPT controller. The system components used in the simulation are show in Table 3.1. These parameters are derived from VELOX-I nano-satellite and is used as an illustrative example for this thesis. For simplification of the simulation, the PV parameters in Table 3.1 are the PV configuration for two series and one parallel instead of two series and four parallel.

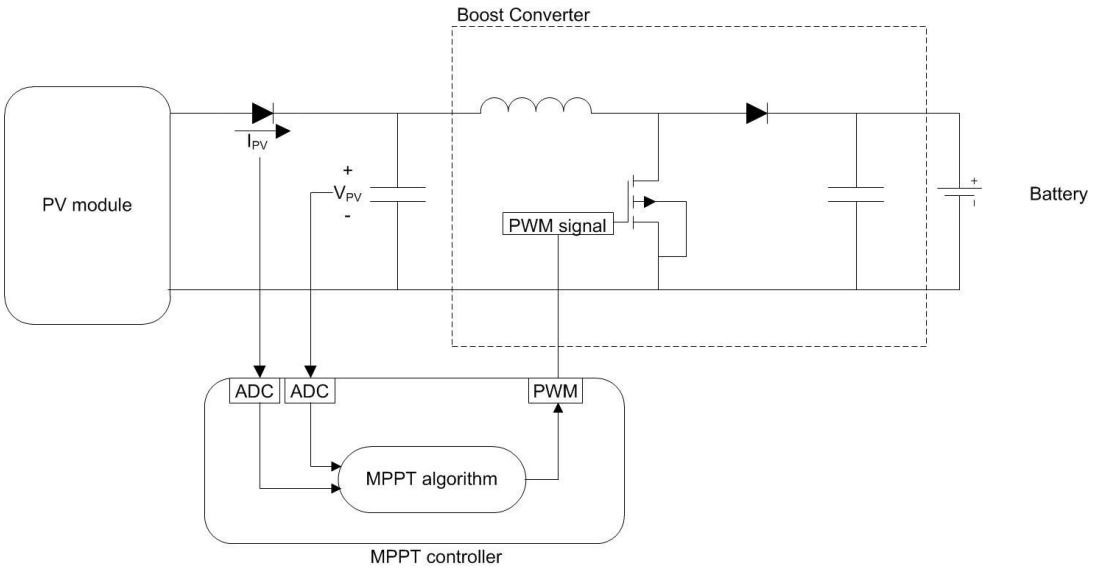

Fig. 3.1 Block diagram of system used to evaluate MPPT methods

Table 3.1 Parameters of components used in PV system

PV array	Open circuit voltage	5.338 V (at T = 28 °C)
	Short circuit current	0.525 A (at T = 28 °C)
	Maximum power	2.4W (at T = 28 °C)
Boost converter	Inductor	330 μH
	MOSFET switching frequency	30 kHz
	Capacitor	470 μF
Battery	Maximum voltage	8.4 V
	Capacity	5.4 Ah

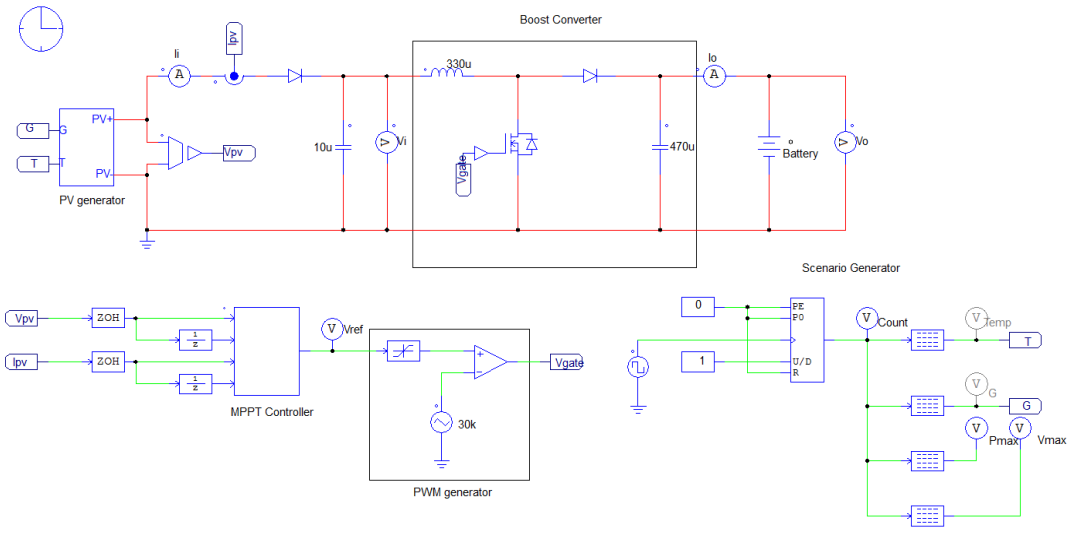

Fig. 3.2 PSIM simulation model of PV system with conventional MPPT

The system is simulated using PSIM software as shown in Fig. 3.2. In the simulation, the orbit profile with PV temperature and solar insolation is updated every second in the simulation. The sampling time of MPPT controller is chosen to be 0.5 seconds. Under the same scenario, different MPPT techniques with different step change of duty cycle (ΔD) ranging from 1% to 5% have been simulated. Two conventional MPPT methods namely the P&O and InC methods have been implemented for the MPPT controller in the simulation.

The performance of MPPT methods under two satellite scenario, normal operating mode and safe-hold operating mode are studied and evaluated. During the normal operating mode, all the subsystems in the satellite are in operation. On the other hand, in the event of a subsystem malfunction, the satellite will enter the safe-hold operating mode. In normal operating mode, the satellite will constantly track the Sun with attitude determination and control system (ADCS). If there is a sudden failure of ADCS, the satellite will lost its stabilization and start to tumble in safe-hold operating

mode. Thus, the satellite will experience certain degree of rotations. The four scenarios used in this study are shown in Fig. 3.3.

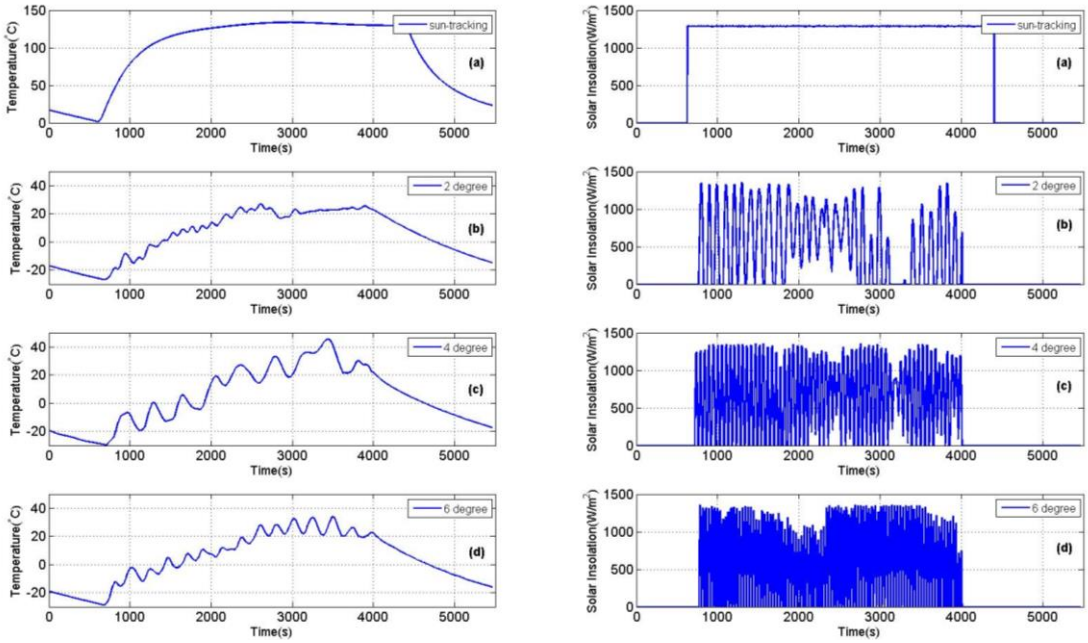

Fig. 3.3 Temperature and solar insolation level profile for satellite under different scenarios (a) normal operating mode with sun-tracking (b) safe-hold operating mode with 2 degrees/s rotation (c) safe-hold operating mode with 4 degree/s rotation (d) safe-hold operating mode with 6 degree/s rotation

Fig. 3.3 shows the temperature and solar insolation level profile for different satellite scenarios. The profile is generated based on a series of simulations [45]. The first step is to conduct the satellite attitude simulation based on various rotation rates. For the simulation, the sun model and the actual satellite's two-line element (TLE) are used. Moreover, the sun incident angle towards each PV panel under different rotation rates of the satellite are calculated and used later to obtain the temperature of the PV panels. This is done by using the finite element model of the satellite in SolidWorks. The solar absorptivity and infrared emissivity of actual PV panels are used in the thermal simulation.

For a satellite flying in the normal operating mode, the PV array of the satellite is constantly facing the Sun. Thus, it is observed that the solar insolation level is staying at constant value as the satellite is performing sun pointing. Meanwhile, the PV temperature tends to be higher as compare to the safe-hold operating scenarios. For satellite safe-hold operating scenarios, it is assumed that the satellite will experience 2 degree, 4 degree and 6 degree per second of rotations. During the safe-hold scenarios, it is clearly seen that the PV temperature is fluctuating within 1°C every second and the solar insolation level changes rapidly as the satellite rotates faster. The rate of change of temperature and solar insolation level in second are plotted in Fig. 3.4.

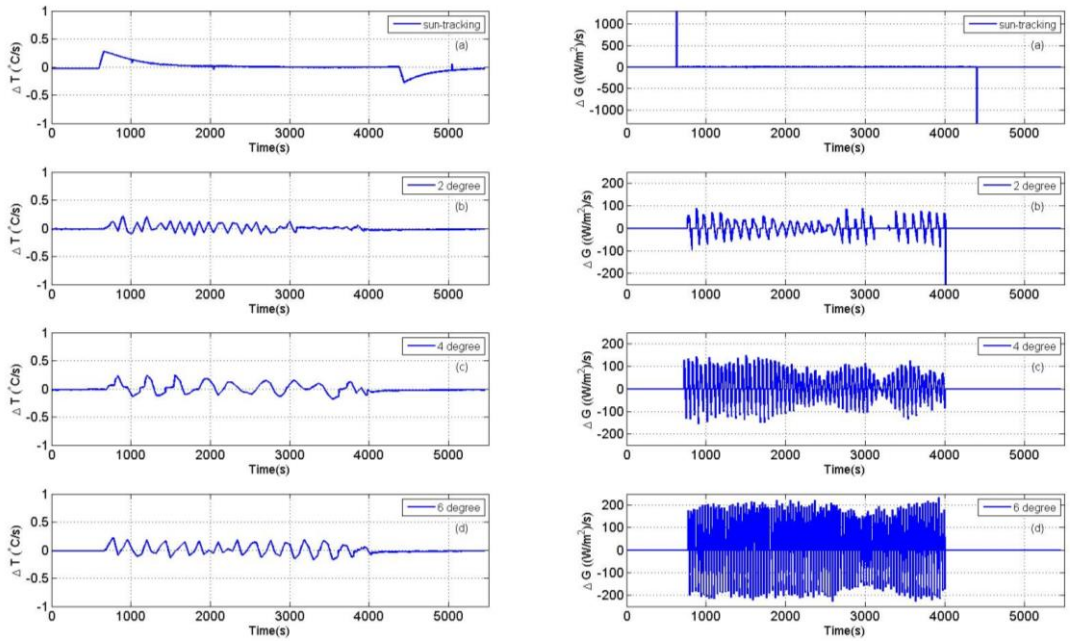

Fig. 3.4 Rate of change of temperature and solar insolation level for satellite under different scenarios (a) normal operating mode with sun-tracking (b) safe-hold operating mode with 2 degrees/s rotation (c) safe-hold operating mode with 4 degree/s rotation (d) safe-hold operating mode with 6 degree/s rotation

3.2. **Analysis and Evaluation of Simulation Study**

The performance of MPPT techniques are compared in terms of tracking efficiency and tracking error. The tracking efficiency (η) is defined as below:

$$\eta = \frac{\int_0^T V_{PV}(t)\, I_{PV}(t) dt}{\int_0^T P_{\max}(t)\, dt} \times 100\% \tag{3.1}$$

where

$V_{PV}(t)$: sampled PV array voltage in orbit period

$I_{PV}(t)$: sampled PV array current in orbit period

$P_{max}(t)$: maximum power provided by PV array

T : total orbit period

dt : sampling time

The tracking efficiency in (3.1) indicates how well the MPPT algorithm tracks the environmental changes [21].

3.2.1. **Normal operating mode**

During the normal operating mode, the solar insolation level and temperature in Fig. 3.3(a) is used in the PSIM-based simulation program in Fig. 3.2. With the temperature and solar insolation level scenario in Fig. 3.3(a), the theoretical maximum power, P_{max} is solved using *I-V* equation in (2.3). The solar array output tracked power is produced by PSIM-based simulation and the result is plotted in Fig. 3.5.

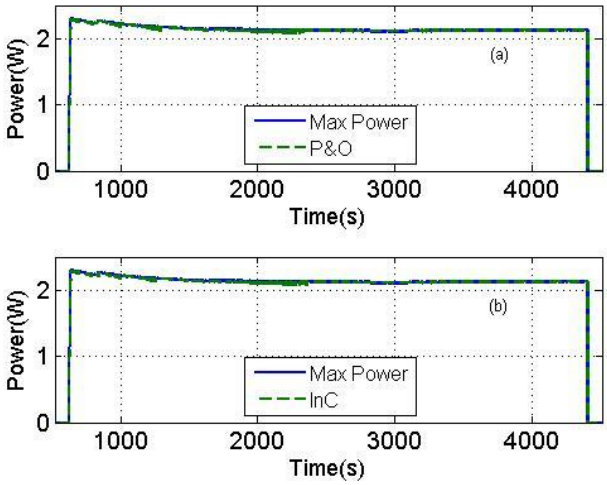

Fig. 3.5 Simulated PV output power during the normal operating mode with conventional MPPT algorithm with 1% perturbation size (ΔD) (a) P&O (b) InC

Fig. 3.5 shows the maximum power and the solar array output power tracking with conventional MPPT methods in the simulation. From Fig. 3.5, the mean error of tracking power for P&O and InC method with 1% perturbation size are 10.4 mW and 10.1 mW respectively. This shows that the performance of both conventional methods are similar. The simulation has been conducted for different perturbation size from 1% to 5% and its tracking efficiency is calculated using (3.1). The tracking efficiency of both MPPT methods with different perturbation size under satellite normal operating scenario is plotted in Fig. 3.6.

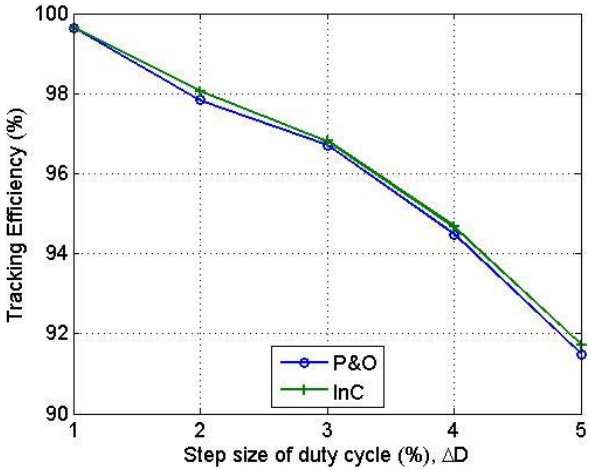

Fig. 3.6 Tracking efficiency of P&O and InC during the normal operating mode

From Fig. 3.6, it is observed that the tracking efficiency is affected by the change of perturbation size. In varying the perturbation size, the smaller size give better tracking performance under normal operation scenario. Both the conventional MPPT methods give above 90% tracking performance for different perturbation size. InC method has a slightly better performance than P&O method in all cases. From Fig. 3.6, it is observed that as the perturbation size increases from 1% to 5%, the tracking efficiency of both MPPT methods decreases from 99% to 91%. As seen in Fig. 3.7 and Fig. 3.8, this is due to the oscillation at the steady state where the tracking is close to maximum power point (MPP).

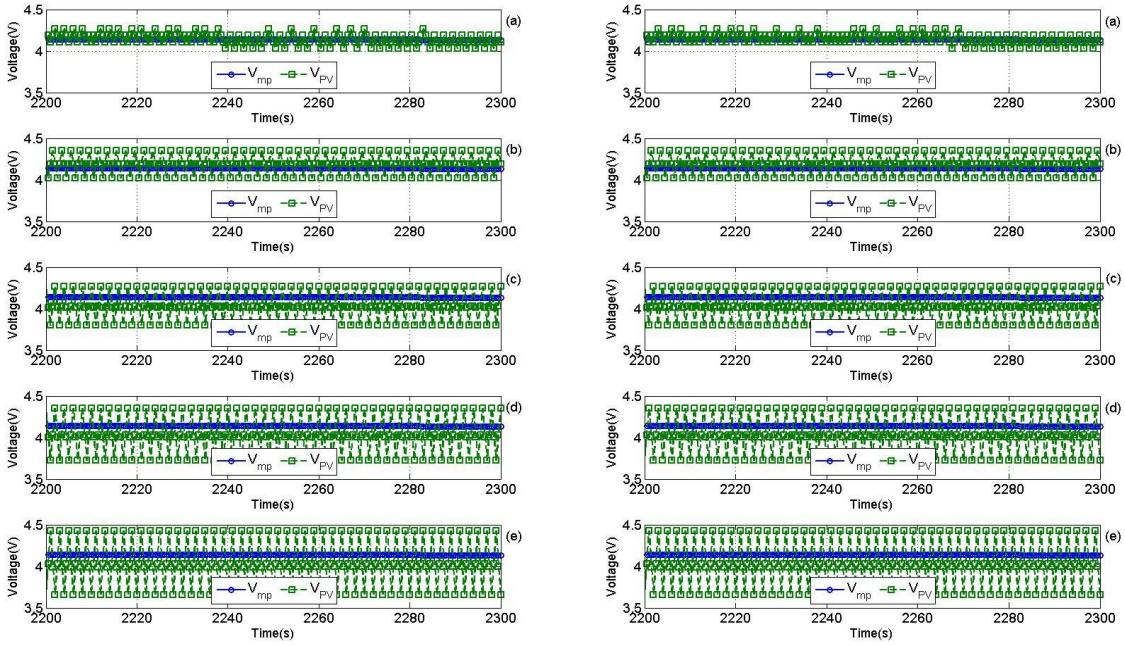

Fig. 3.7 PV operating point oscillation at steady state with P&O (left) and InC (right) with ΔD (a) 1% (b) 2% (c) 3% (d) 4% (e) 5% during the normal operating mode

Fig. 3.7 shows the PV operating voltage (V_{PV}) is oscillating around the maximum power point voltage (V_{mp}). During the normal operating mode, the V_{mp} will remain almost constant. However, the conventional MPPT methods have drawback of steady-state oscillation. As the perturbation size increases, the oscillation tends to be larger. The oscillation effect in Fig. 3.7 will incur the power loss as shown in Fig. 3.8.

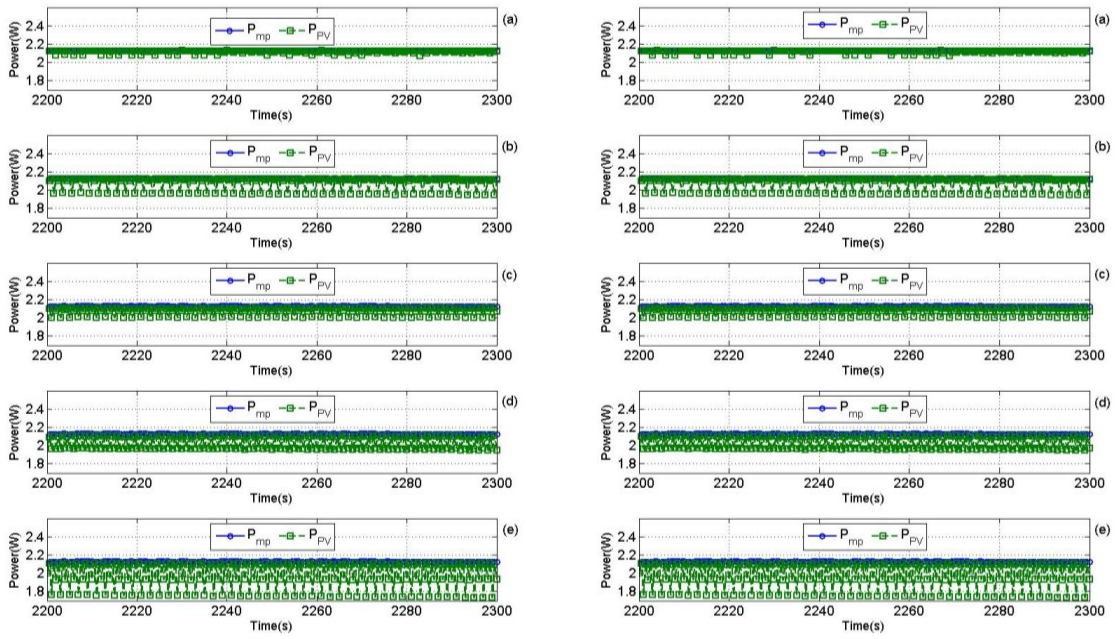

Fig. 3.8 Tracking power loss at steady-state oscillation, P&O (left) and InC (right) with ΔD (a) 1% (b) 2% (c) 3% (d) 4% (e) 5% under normal operation scenario

Fig. 3.8 shows the tracked power of the PV in the steady state. It can be clearly seen that larger perturbation size leads to larger power loss and thus reduces the tracking efficiency. During normal operating scenarios, the satellite will experience stable environmental condition. Thus, it will experience steady-state oscillation at most of the time. Therefore, it is recommended to use a smaller perturbation size for the normal operating mode.

3.2.2. **Safe-hold operating mode**

From previous section, it is concluded that the conventional MPPT methods could perform well in Sun tracking conditions. The tracking performance is limited by its steady-state oscillation effect. Next, their performance will be evaluated using the solar insolation and temperature presented in Fig. 3.3(b)-(d) under safe-hold operating mode.

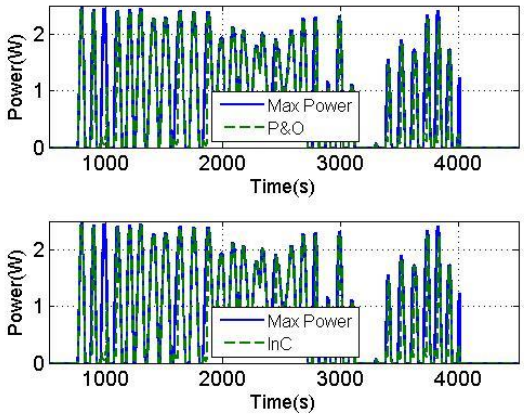

(a) 2 degree rotation scenarios

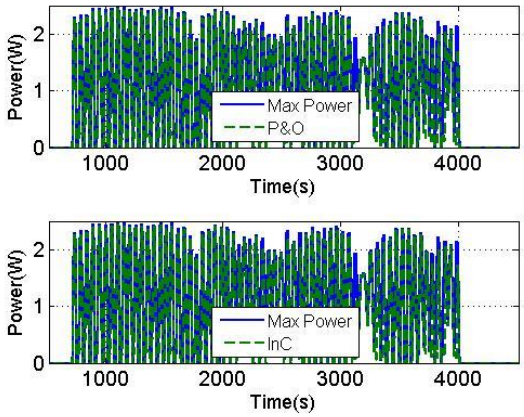

(b) 4 degree rotation scenarios

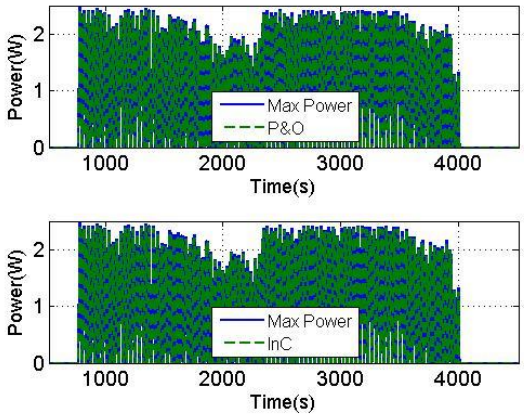

(c) 6 degree/s rotation scenarios

Fig. 3.9 Simulated PV output power under safe-hold operation scenarios with tracking MPPT algorithm with 1% perturbation size (ΔD)

Fig. 3.9 shows the theoretical maximum power and the tracked PV power with conventional MPPT methods in the simulation for safe-hold operation scenarios. When the satellite is in safe-hold operation, the satellite is experiencing rotation. The rotation causes the satellite PV to face the Sun at different angles which constantly change solar insolation level. The simulation has been further conducted with different perturbation size from 1% to 5% and different initial duty cycle from 30% to 70%. The tracking efficiency is calculated and plotted in Fig. 3.10.

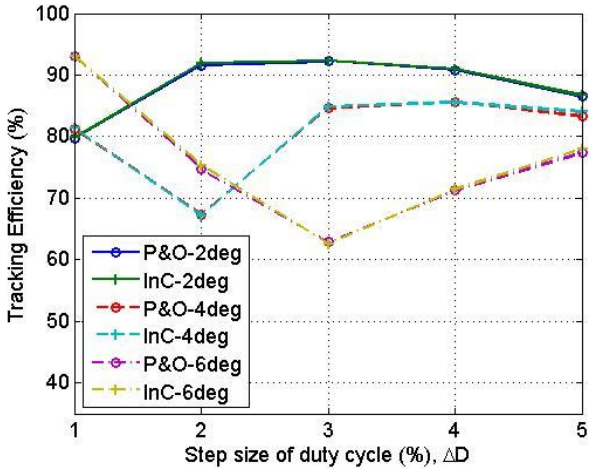

Fig. 3.10 Tracking efficiency of P&O and InC under safe-hold operation scenarios

Fig. 3.10 shows the tracking efficiency along with the step size of duty cycle (ΔD) for the two MPPT techniques under satellite rotation scenarios. Each point represents the statistical mean of nine sets of different initial duty cycle ranging from 30% to 70% in step of 5%. These curve shows that the performance of P&O and InC are similar as the difference of their tracking efficiency is less than 1% in all scenarios with the same step size of duty cycle (ΔD). The results show that the conventional MPPT methods having inconsistent performance with efficiency ranging from 62% to 93% if the satellite is rotating regardless of the perturbation size. Table 3.2

summarizes the tracking efficiency of the conventional MPPT methods for all satellite scenarios.

Table 3.2 Tracking efficiency under satellite scenario with P&O and InC for different ΔD

	Sun tracking		2 degree/s rotation		4 degree/s rotation		6 degree/s rotation	
	Average Tracking Error (W)	Tracking Efficiency (%)	Average Tracking Error (W)	Tracking Efficiency (%)	Average Tracking Error (W)	Tracking Efficiency (%)	Average Tracking Error (W)	Tracking Efficiency (%)
P&O								
ΔD = 1%	**0.0104**	**99.64**	0.2667	79.76	0.2484	81.26	**0.0942**	**93.01**
ΔD = 2%	0.0483	97.84	0.1125	91.61	0.4344	67.40	0.3415	74.72
ΔD = 3%	0.0706	96.71	**0.1032**	**92.28**	0.2064	84.65	0.5054	62.85
ΔD = 4%	0.1172	94.48	0.1296	90.83	**0.1987**	**85.64**	0.3898	71.27
ΔD = 5%	0.1795	91.49	0.1842	86.50	0.2167	83.28	0.3082	77.40
InC								
ΔD = 1%	**0.0101**	**99.64**	0.2660	79.81	0.2466	81.32	**0.0944**	**93.00**
ΔD = 2%	0.0438	98.05	0.1086	91.93	0.4367	67.20	0.3327	75.39
ΔD = 3%	0.0686	96.81	**0.1031**	**92.34**	0.2035	84.86	0.5094	62.57
ΔD = 4%	0.1135	94.67	0.1262	91.03	**0.2007**	**85.56**	0.3884	71.45
ΔD = 5%	0.1751	91.72	0.1670	86.74	0.2038	84.00	0.2984	77.98

From Table 3.2, it is observed that the smaller perturbation size give the best tracking performance in the satellite normal operation scenarios but not in the satellite safe-hold operation scenarios. Besides that, both the conventional MPPT methods have poorer tracking performance in the satellite safe-hold operation scenarios as compared to the satellite normal operation scenarios. The main reason for the poor MPPT performance in the satellite safe-hold operation scenarios is that the PV will experience rapid change of environment while the satellite is rotating in space. For conventional MPPT methods, it requires two pairs of voltage and current measurements. During satellite safe-hold operation scenarios, the measurements may occur at different temperature and solar insolation level. Thus, this leads the P&O and InC methods to perturb in wrong direction resulting PV operating point drift away from MPP.

3.3. **Summary**

In this chapter, a simulation study for a satellite using P&O and InC methods to achieve peak power tracking has been conducted. From the results, it is observed that both P&O and InC methods perform well when the satellite is performing Sun tracking scenario with small perturbation size. Although smaller perturbation size gives slower respond, it leads to lesser oscillation in the steady state and better tracking performance. When the satellite is experiencing rotation, the performance of the conventional MPPT methods is inconsistent as the tracking efficiency can decrease up to 35%.

To overcome the shortcomings of P&O and InC methods in satellite application, a new tracking method will be proposed in the next chapter that attempts to achieve better performance in both normal operation and safe-hold operation.

CHAPTER 4. SOLAR INSOLATION AND MAXIMUM POWER POINT ESTIMATION (SIMPPE)

The simulation results presented in Chapter 3 demonstrated that the conventional maximum power point tracking (MPPT) methods do not perform well when the satellite is operating under safe-hold operation. The main reason is due to the change of solar insolation level of the photovoltaic (PV) array causes the maximum power point (MPP) change when the satellite undergoes rotation. To address this shortcoming, a new model based MPPT algorithm with solar insolation level estimation is proposed and presented in this chapter.

Every PV array has a unique MPP for a given temperature and solar insolation level. A PV model can be used to estimate the actual *I-V* characteristic if the values of the equivalent circuit parameters are known. Usually, the parameters such as short circuit current ($I_{sc,n}$), open circuit voltage ($V_{oc,n}$), voltage at MPP ($V_{mp,n}$), current at MPP ($I_{mp,n}$), open circuit voltage thermal coefficient (K_v) and short circuit current thermal coefficient (K_i) at standard test conditions (STC) are given in the data sheet. With these parameters, it is possible to identify the equivalent circuit parameters, namely the diode ideality factor (a), series resistance (R_s) and parallel resistance (R_p) using the particle swarm optimization (PSO) algorithm in [38]. With the PV model known, the next step is to develop a model based MPPT.

To implement a model based MPPT, the information of environmental conditions such as temperature and solar insolation level are required. The measurement of PV cell temperature can be implemented using the thermocouples that are capable of

measuring a wide range of temperature. To measure solar insolation level, the pyranometer is the typical sensor used.

Model based MPPT [46, 47] has shown the advantage of dynamic response in rapidly changing conditions. In addition, it solves the steady-state oscillation issue faced by the P&O and InC methods. Moreover, it does not require training data such as the artificial neural network (ANN) which is not feasible for space application.

The model based MPPT method in [46] is able to eliminate the needs of pyranometer by estimate the solar insolation with an adequate accuracy. This reduces the cost while maintaining a good accuracy in tracking of the MPP. The main drawback in [46] is its requirement of the PV parameters to compute through experimental data. In space, the PV suffers high degradation as compared to PV on Earth. Thus, the parameters obtained through experiment may not be accurate after the satellite is orbiting in space.

The proposed method in [47] solves for *I-V* curve instead of estimating temperature and solar insolation using a single-diode and four-parameter model. In [47], it introduced some conditions to ensure that the estimated *I-V* curve is valid. However, this method only works when the PV's operating point is near the MPP. Thus, it required the P&O to find the first MPP which will be used in the proposed method in [47].

In the next section, a model based MPPT method with solar insolation and MPP estimation (SIMPPE) procedure will be introduced. Different from the reported approaches, the information of solar insolation level can be predicted using an offline PV model and real time PV measurements. Using the single diode PV model, the

estimation of solar insolation level is formulated with the knowledge of voltage, current and temperature measured from the PV array. The SIMPPE algorithm tracks the MPP with the estimated solar insolation level and measured temperature. The SIMPPE has been validated using simulation and experimental studies. The simulation studies are conducted under various environmental conditions and different levels of sensing errors to analyse its feasibility. The performance of the SIMPPE algorithm will be verified using the same PSIM-based simulation and operation scenarios from Chapter 3. Finally, the SIMPPE algorithm has been validated experimentally.

4.1. **SIMPPE Algorithm**

For the SIMPPE algorithm, a single diode model is considered due to its accuracy and simplicity [48]. In order to track the MPP of the PV, it is first necessary to identify the PV model parameters, namely the diode ideality factor (a), series resistance (R_s) and parallel resistance (R_p). From the single diode model in Fig. 2.1, the PV array output current is expressed as

$$I = I_{ph} - I_{rs}\left[\exp\left(\frac{V + R_s I}{a N_s V_t}\right) - 1\right] - \frac{V + R_s I}{R_p} \tag{4.1}$$

In (4.1), the unknown parameters to be solved are I_{ph}, I_{rs}, a, R_s and R_p. In [39], the solution of I_{ph} and I_{rs} are given as

$$I_{ph} = \left(I_{ph,n} + K_i \Delta T\right)\frac{G}{G_n} \tag{4.2}$$

$$I_{rs} = \frac{I_{sc,n} + K_i \Delta T}{\exp\left(\frac{\mathrm{V}_{oc,n} + K_v \Delta T}{a\,\mathrm{N}_s\, V_t}\right) - 1} \tag{4.3}$$

where

$I_{ph,n}$: nominal generated photo current

K_i : short circuit current temperature coefficient

ΔT : different between actual temperature and nominal temperature, ($T - T_n$)

G : solar insolation on the solar panel

G_n : nominal solar insolation

$I_{sc,n}$: short circuit current at nominal condition

$V_{oc,n}$: open circuit voltage at nominal condition

K_v : open circuit voltage temperature coefficient

The solution of nominal generated photo current $I_{ph,n}$ can be obtained by rewriting (4.1) under the condition of short circuit ($I = I_{sc,n}$, $V = 0$) at nominal STC condition as

$$I_{sc,n} = I_{ph,n} - I_{rs}\left[\exp\left(\frac{R_s I_{sc,n}}{aN_s V_t}\right) - 1\right] - \frac{R_s I_{sc,n}}{R_p} \tag{4.4}$$

Under short circuit condition, the reverse saturation current can be neglected in (4.4) [39, 48]. Thus, (4.4) can be simplified as

$$I_{ph,n} = \frac{R_p + R_s}{R_p} I_{sc,n} \tag{4.5}$$

Substituting (4.5) into (4.2) yields

$$I_{ph} = \left(\frac{R_p + R_s}{R_p} I_{sc,n} + K_i \Delta T\right)\frac{G}{G_n} \tag{4.6}$$

By substituting (4.3) and (4.6) into (4.1), the equation can be rewritten as

$$I = \left(\frac{R_p + R_s}{R_p} I_{sc,n} + K_i \Delta T \right) \frac{G}{G_n} - \frac{I_{sc,n} + K_i \Delta T}{\exp\left(\frac{V_{oc,n} + K_v \Delta T}{a N_s V_t} \right) - 1} \left[\exp\left(\frac{V + R_s I}{a N_s V_t} \right) - 1 \right] - \frac{V + R_s I}{R_p} \tag{4.7}$$

Most of the PV array manufacturers provide the PV array information with reference to nominal condition of temperature and solar insolation level. Therefore, the information of $I_{sc,n}$, $V_{oc,n}$, K_i, K_v and G_n are available in PV array datasheets.

The unknown parameters a, R_s and R_p are temperature dependent variables. They can be obtained using the PSO algorithm [38]. To implement real-time PSO algorithm, the code size is large and time consuming. Thus, an alternative solution is to solve the parameters a, R_s and R_p offline and stored them in a lookup table.

With a, R_s and R_p known, the only unknown parameter is the solar insolation which can be estimated together with the three measurement readings ($\tilde{V}, \tilde{I}, \tilde{T}$). Thus, (4.7) can be rewritten as follow to estimate the solar insolation.

$$G_{est} = \frac{\tilde{I} + \frac{I_{sc,n} + K_i \Delta \tilde{T}}{\exp\left(\frac{V_{oc,n} + K_v \Delta \tilde{T}}{a N_s V_t(\tilde{T})} \right) - 1} \left[\exp\left(\frac{\tilde{V} + R_s \tilde{I}}{a N_s V_t(\tilde{T})} \right) - 1 \right] + \frac{\tilde{V} + R_s \tilde{I}}{R_p}}{\frac{R_p + R_s}{R_p} I_{sc,n} + K_i \Delta \tilde{T}} \times G_n \tag{4.8}$$

With G_{est}, $\tilde{T}$, a, R_s, and R_p, the I-V curve can be estimated by solving $I = f(V, I)$. Once the I-V curve is estimated, the MPP can be calculated. The transcendental equation, $I = f(V, I)$ can be solved by numerical methods such as Newton-Raphson method. An overview of the SIMPPE algorithm is shown in Algorithm 4.1.

Step 1: Measure PV voltage, current and temperature

$$\tilde{V}, \tilde{I}, \tilde{T}$$

Step 2: Initialize a, R_s and R_p from lookup table based on PV measured temperature

Step 3: Solve G_{est} using (4.8)

$$G_{est} = \frac{\tilde{I} + \dfrac{I_{sc,n} + K_i \Delta\tilde{T}}{\exp\left(\dfrac{V_{oc,n} + K_v \Delta\tilde{T}}{a N_s V_t(\tilde{T})}\right) - 1}\left[\exp\left(\dfrac{\tilde{V} + R_s\tilde{I}}{a N_s V_t(\tilde{T})}\right) - 1\right] + \dfrac{\tilde{V} + R_s\tilde{I}}{R_p}}{\dfrac{R_p + R_s}{R_p} I_{sc,n} + K_i \Delta\tilde{T}} \times G_n$$

Step 4: Recursively solve the following equation $I = f(V, I)$, for $0 \le V \le V_{oc}$

$$I = I_{ph} - I_{rs}\left[\exp\left(\frac{V + R_s I}{a N_s V_t}\right) - 1\right] - \frac{V + R_s I}{R_p}$$

Step 5: Find V_{mp} by calculate P for $0 \le V \le V_{oc}$

Algorithm 4.1 Proposed SIMPPE algorithm

As illustrated in Algorithm 4.1, the PV voltage, current and temperature are first measured. With the PV temperature measurement, the PV temperature dependent parameters (a, R_s, R_p) can be extracted using a lookup table where the values have been obtained offline using the PSO algorithm. The solar insolation can be estimated using the PV model along with PV measurements and other parameters using (4.8). Using the PV model, the *I-V* curve can next be generated using the PV temperature measurement and estimated solar insolation. The generated *I-V* curve can then be used to identify the MPP of the PV array.

4.2. **Feasibility Studies of SIMPPE Algorithm**

Based on the SIMPPE algorithm, the feasibility of the algorithm is first investigated. A simulation study has been conducted using MATLAB to evaluate the feasibility of the SIMPPE algorithm for PV operating at different PV operating points.

For the simulation study, the PV parameters is configured based on Azur Space solar cell and its specification is given in Table 4.1.

Table 4.1 PV parameters for simulation study (Azur Space TJ Solar Cell 3G30C)

Nominal open circuit voltage, $V_{oc,n}$	5.338V (at T = 28 °C)
Nominal short circuit current, $I_{sc,n}$	0.525A (at T = 28 °C)
Nominal maximum power, $P_{mp,n}$	2.4W (at T = 28 °C)
Open circuit voltage temperature coefficient, K_v	- 6mV/°C
Short circuit current temperature coefficient, K_i	0.32mA/°C

In [38], the PSO algorithm is used to solve the PV temperature dependent parameters (a, R_s, R_p) at different temperatures with the PV parameters given in Table 4.1. Thus, the simulation is able to generate the *I-V* curves at different temperatures and solar insolation using (4.7). Each *I-V* curve has 200 points of voltage and current readings that will be used in the SIMPPE algorithm to estimate solar insolation level and MPP voltage. The solar insolation level estimation and MPP voltage estimation results are shown in Fig. 4.1 and Fig. 4.2 respectively.

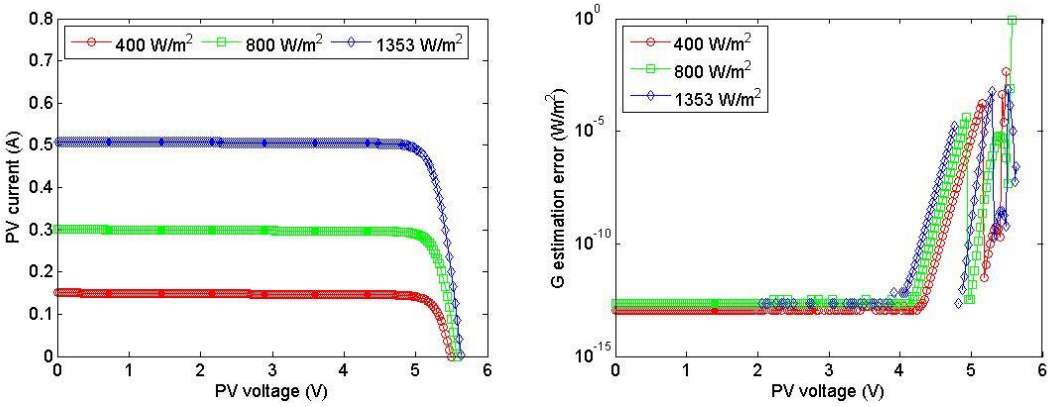

(a) T = -22°C

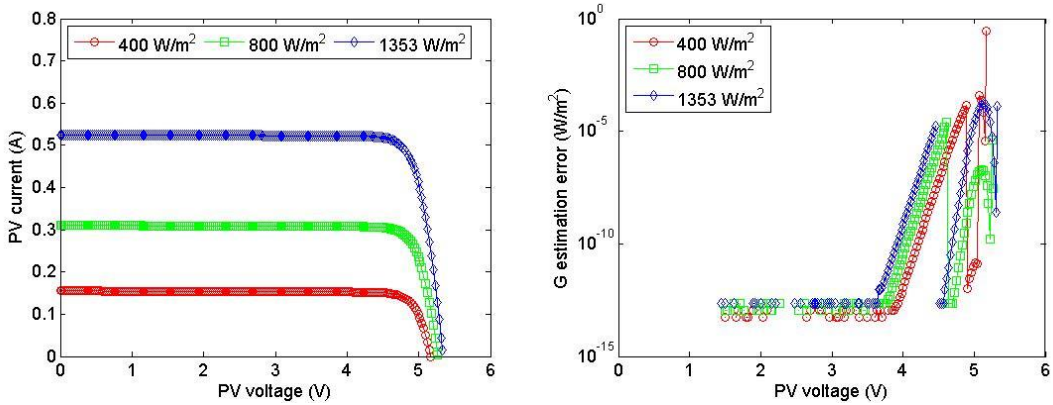

(b) T = 28°C

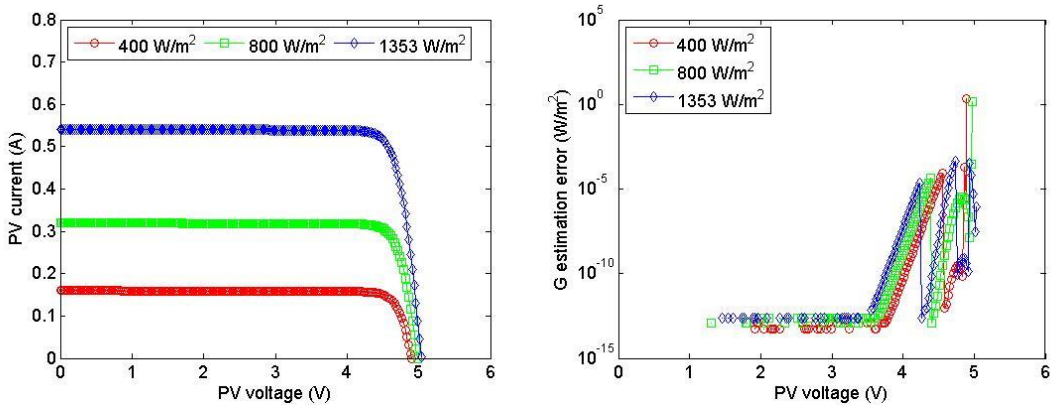

(c) T = 78°C

Fig. 4.1 PV *I-V* curve (left) and error of solar insolation level estimation (right) under different temperatures and solar insolation level conditions

Fig. 4.1 shows the *I-V* curves that obtained from [38] under different temperature conditions (T = -22°C, 28°C, 78°C) and solar insolation level conditions (G = 400W/m^2, 800W/m^2, 1353W/m^2) which are within the range based on LEO satellite operation. This is to study the influence of the location of the measured voltage and current pair in performing accurate solar insolation level estimation. The markers in left of Fig. 4.1 denote the 200 points of voltage and current readings that are used to estimate the solar insolation level with PV temperature using (4.8). The solar insolation estimation errors are the markers in the right of Fig. 4.1. Generally, when

the solar insolation is low, the SIMPPE algorithm gives a higher estimation error as compared to higher solar insolation level. Under low solar insolation level (400W/m^2) scenario, the maximum solar insolation level estimation relative error is less than 1%, which is below 4W/m^2. Due to the limitation of single diode model [49], the accuracy of the single diode PV model deteriorates when approaching open circuit voltage.

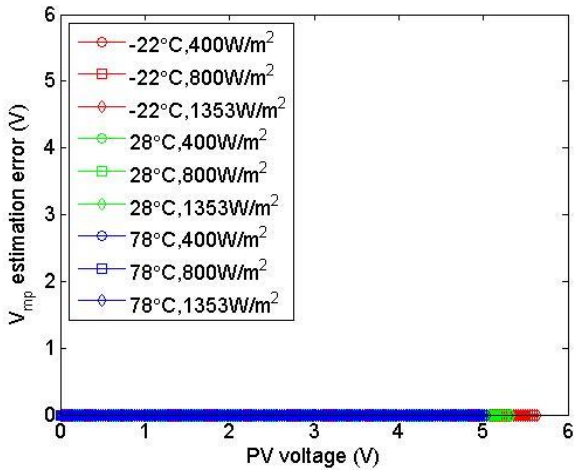

Fig. 4.2 Error of V_{mp} estimation and solar insolation level estimation under different temperature and solar insolation level conditions

Fig. 4.2 shows the relationship of solar insolation level estimation and V_{mp} estimation errors under different temperature conditions (T = -22°C, 28°C, 78°C) and solar insolation level conditions (G = 400W/m^2, 800W/m^2, 1353W/m^2). From Fig. 4.2, with the small solar insolation estimation relative error of less than 1%, the single diode PV model can give an accurate estimation of V_{mp} which leads to good tracking efficiency. This shows that the location of measured pair will not affect the tracking efficiency. Table 4.2 summarizes the results of Fig. 4.1 and Fig. 4.2.

Table 4.2 Summary of solar insolation estimation and MPP estimation

Scenarios	Mean G estimation absolute error (W/m^2)	Maximum G estimation absolute error (W/m^2)	Mean V_{mp} estimation absolute error (V)
T = -22°C, G = 400W/m^2	1.332 x 10^{-4}	0.0043	0
T = -22°C, G = 800W/m^2	0.0122	0.8187	0
T = -22°C, G = 1353W/m^2	9.4078 x 10^{-4}	7.3577 x 10^{-4}	0
T = 28°C, G = 400W/m^2	0.0097	0.2795	0
T = 28°C, G = 800W/m^2	3.198 x 10^{-7}	2.5844 x 10^{-5}	0
T = 28°C, G = 1353W/m^2	5.2947 x 10^{-6}	1.6091 x 10^{-4}	0
T = 78°C, G = 400W/m^2	0.0671	2.2478	0
T = 78°C, G = 800W/m^2	0.0217	1.4511	0
T = 78°C, G = 1353W/m^2	6.3604 x 10^{-6}	4.586 x 10^{-4}	0

The simulation study have been extended for different temperature ranging between –30°C and 150°C in step of 1°C. For each temperature, the solar insolation level, G will be set to different solar insolation level (G = 400W/m^2, 800W/m^2, 1353W/m^2). Each generated I-V curve has 200 points of voltage and current measurement pairs that are used to estimate the solar insolation level. This demonstrates the feasibility of SIMPPE algorithm regardless of PV cell temperature.

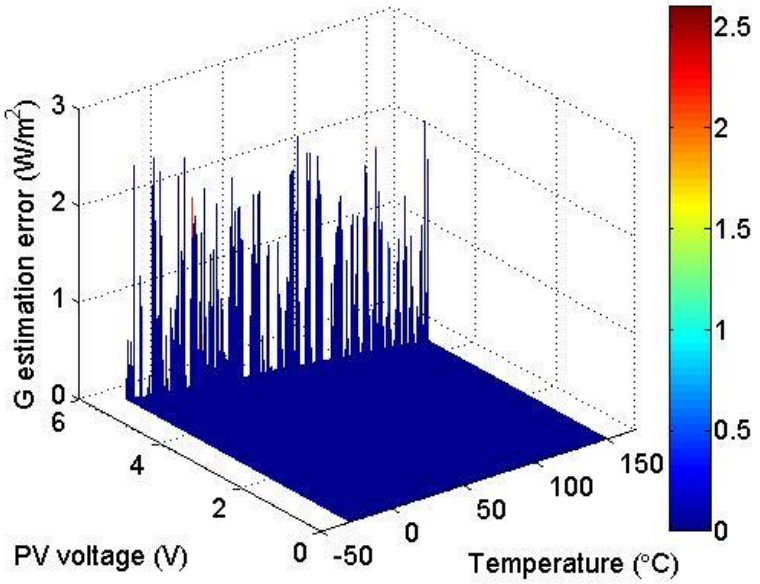

(a) G = 400 W/m^2

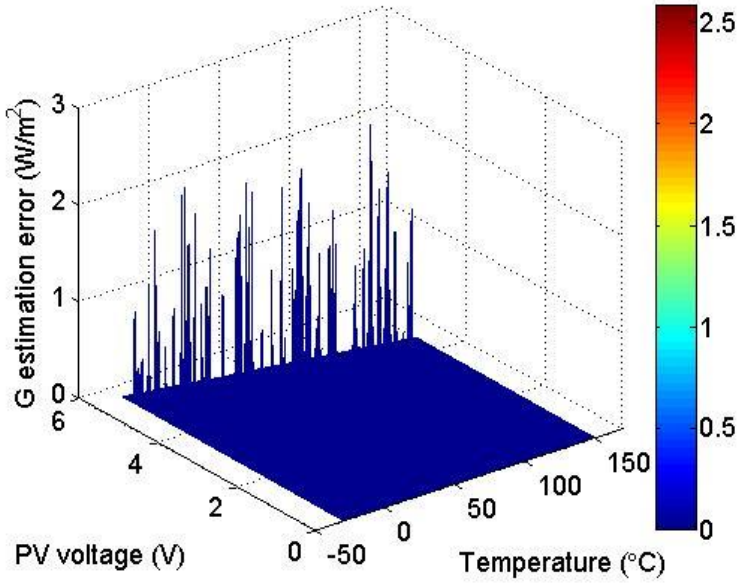

(b) G = 800 W/m^2

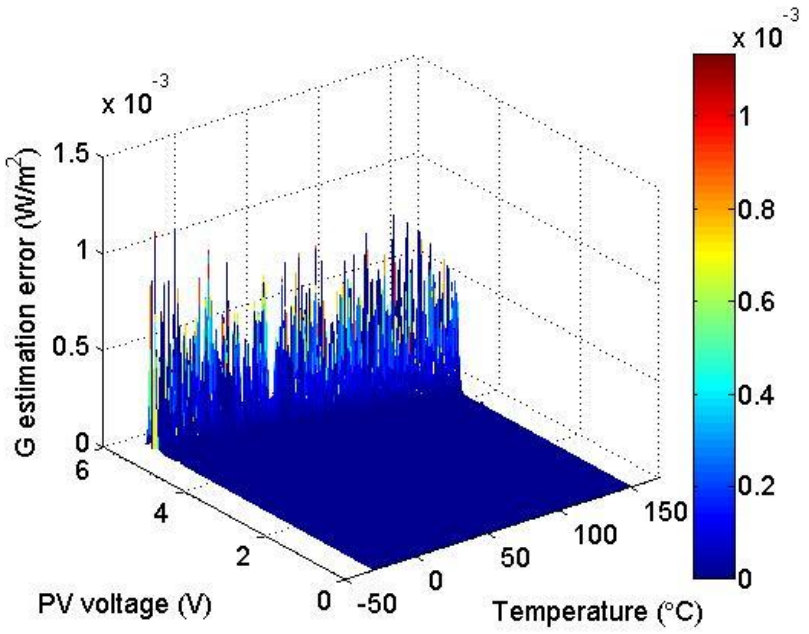

(c) G = 1353 W/m^2

Fig. 4.3 Solar insolation level estimation error under different voltage and temperature

Fig. 4.3 shows the solar insolation level estimation error under varying voltage and temperature at different solar insolation levels, i.e. G = 400W/m^2, 800W/m^2 and 1353W/m^2. From Fig. 4.3, it is observed that solar insolation level estimation errors are larger when the location of voltage and current measurement pair approaching the open circuit voltage at different solar insolation levels. The maximum solar insolation level estimation error remains below 2.5W/m^2 at three different solar insolation level scenarios.

To study the feasibility of the proposed approach in space scenario further, the simulation is run for *I-V* curve generated under different temperature, T and solar insolation level, G. The range of temperature is set between – 30°C and 150°C in step of 1°C while the range of solar insolation level is set between 1W/m^2 and 1353W/m^2 in step of 1W/m^2.

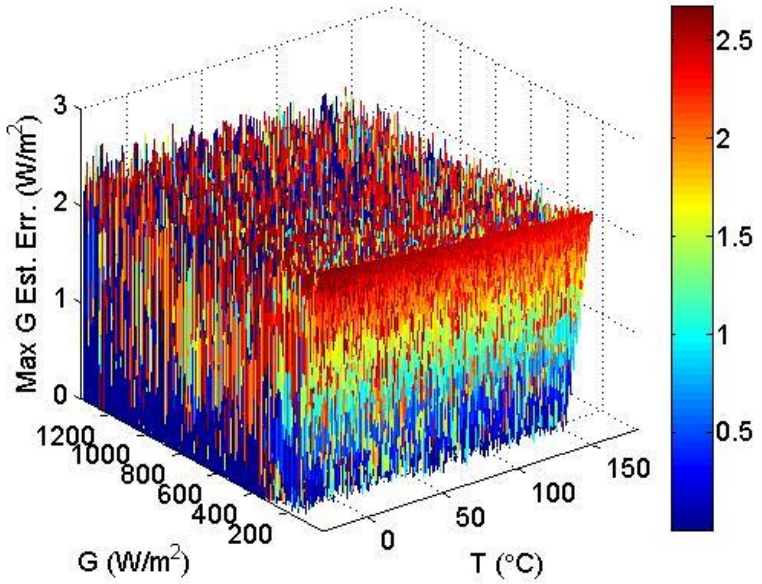

Fig. 4.4 Maximum solar insolation level estimation error under different temperature and solar insolation level

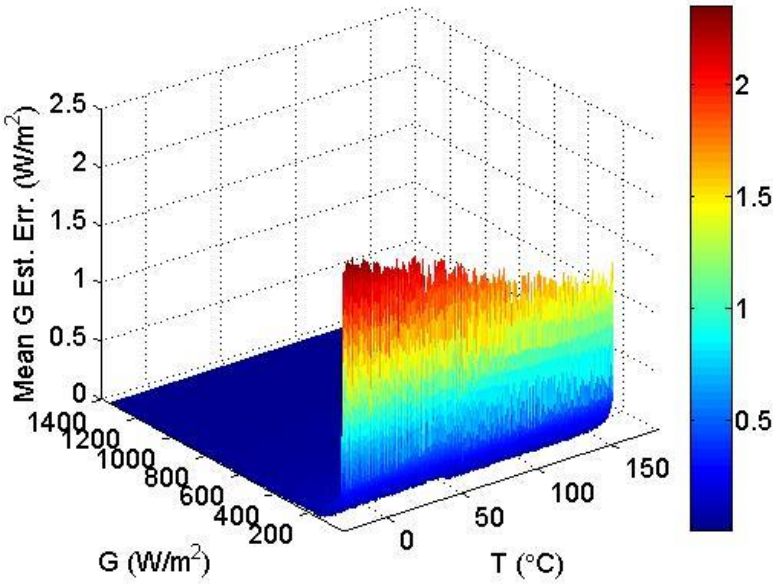

Fig. 4.5 Mean solar insolation level estimation error under different temperature and solar insolation level

Fig. 4.4 shows the absolute maximum of solar insolation level estimation error and Fig. 4.5 shows the mean of solar insolation level estimation error for every *I-V* curve generated under different temperature and solar insolation level scenarios. Each *I-V* curve has 200 pairs of voltage and current measurements that are used to evaluate the performance of the SIMPPE algorithm. The maximum absolute errors and mean absolute errors are calculated as follows:

$$Maximum = Max\left|G_{est}(k) - G_{actual}(k)\right| \tag{4.9}$$

$$Mean = \frac{1}{n}\sum_{k=1}^{n}\left|G_{est}(k) - G_{actual}(k)\right| \tag{4.10}$$

The result in Fig. 4.4 shows that under the worst-case scenario, the absolute maximum solar insolation level estimation errors are less than $3W/m^2$ under all temperature and solar insolation level scenarios. From Fig. 4.5, it shows that in any measurement point of *I-V* curve, the solar insolation level estimation is accurate and its error is close to $0W/m^2$. As the solar insolation level is reduced, the SIMPPE algorithm loses its accuracy and the solar insolation level estimation error rises.

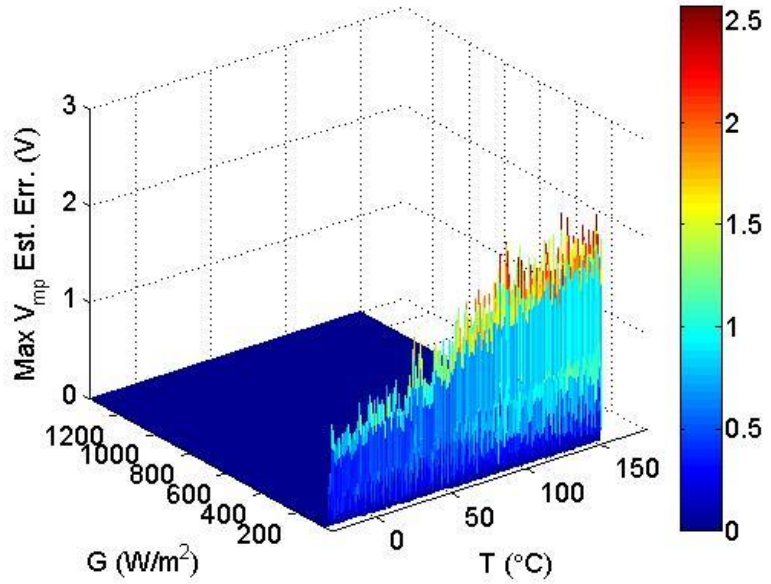

Fig. 4.6 Maximum V_{mp} estimation error under different temperature and solar insolation level

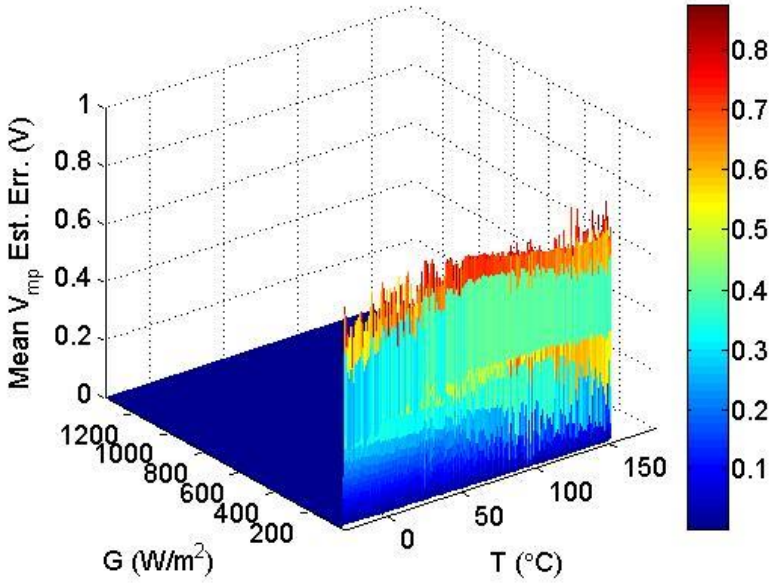

Fig. 4.7 Mean V_{mp} estimation error under different temperature and solar insolation level

Fig. 4.6 shows the maximum of V_{mp} estimation error and Fig. 4.7 shows the mean of V_{mp} estimation error under different temperature and solar insolation level scenarios. The maximum absolute errors and mean absolute errors are calculated as follows:

$$Maximum = Max\left|V_{mp,est}(k) - V_{mp,actual}(k)\right| \tag{4.11}$$

$$Mean = \frac{1}{n}\sum_{k=1}^{n}\left|V_{mp,est}(k) - V_{mp,actual}(k)\right| \tag{4.12}$$

The results in Fig. 4.4-Fig. 4.7 demonstrate that the small solar insolation level estimation error does not affect the V_{mp} estimation. At 95% of temperature and solar insolation level scenarios, the SIMPPE algorithm is able to give accurate V_{mp} estimation where the estimation error is less than 0.05V. The maximum V_{mp} estimation absolute error increases progressively when the solar insolation level is below 40W/m^2. With the V_{mp} estimation, the tracking efficiency is calculated and the worst case of the tracking efficiency is plotted in Fig. 4.8.

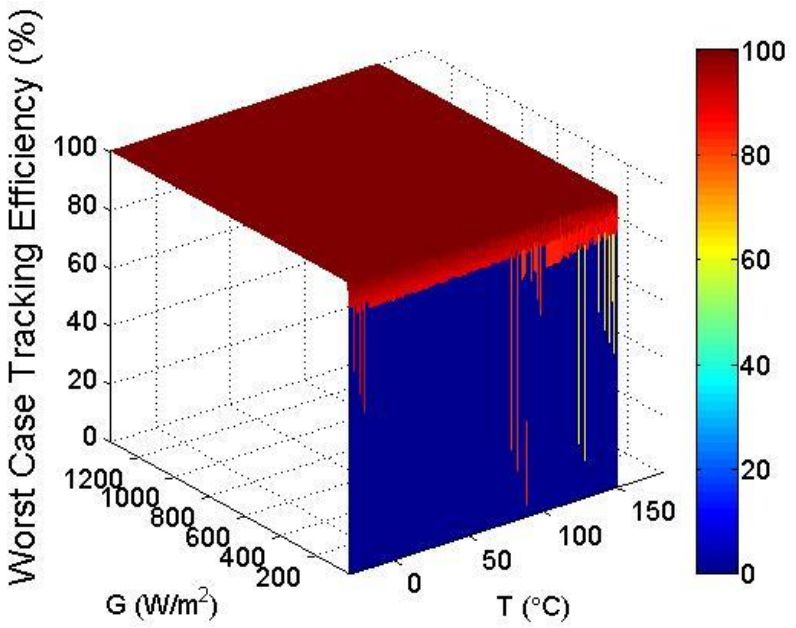

Fig. 4.8 Worst case of tracking efficiency under different temperature and solar insolation level

Fig. 4.8 shows the worst possible case of tracking efficiency under varying temperatures and solar insolation level. From Fig. 4.8, it is observed that temperature condition does not affect the capability of the SIMPPE algorithm in tracking the MPP.

Moreover, the poor tracking performance is only happen during low solar insolation level, where the PV maximum power is low and negligible.

The results in Fig. 4.4-Fig. 4.8 are obtained under ideal scenario without error. In practice, non-ideal case such as measurement noise and quantization error due to ADC have to be taken into consideration For example, a 10-bit ADC is able to give 0.1% of resolution while a 12-bit ADC can give 0.024% of resolution. The quantization error for ADC Simulation study under different resolution of ADC is investigated next of the SIMPPE algorithm. In this simulation study, the measurement range of voltage and current are set to 6V and 1A respectively to cover all the PV voltage and current measurements. The specifications of 10-bit ADC and 12-bit ADC are summarized in Table 4.3.

Table 4.3 ADC specification for microcontroller C8051F12x-13x (P/N: C8051F12x-13x)

	10-bit ADC	12-bit ADC
Measurement Range	0 – 6 V; 0 – 1 A	0 – 6 V; 0 – 1 A
Resolution	6 mV/LSB; 1 mA/LSB (0.1%)	1.44 mV/LSB; 0.24 mA/LSB (0.024%)
Integral Nonlinearity	±1 LSB	±1 LSB
Differential Nonlinearity	±1 LSB	±1 LSB
Offset Error	±0.5 LSB	±1 LSB
Full-Scale Error	±0.5 LSB	±3 LSB

The accuracy of ADC is defined by the total error of ADC. The total error of ADC is equal to the summation of integral nonlinearity error, differential nonlinearity error, offset error and full-scale error from Table 4.3. In the simulation study, the

measurement error is set to randomly ± 18mV / ± 3mA and ± 8.64mV / ± 1.44mA which are equivalent to the total error of 10-bit ADC and 12-bit ADC respectively.

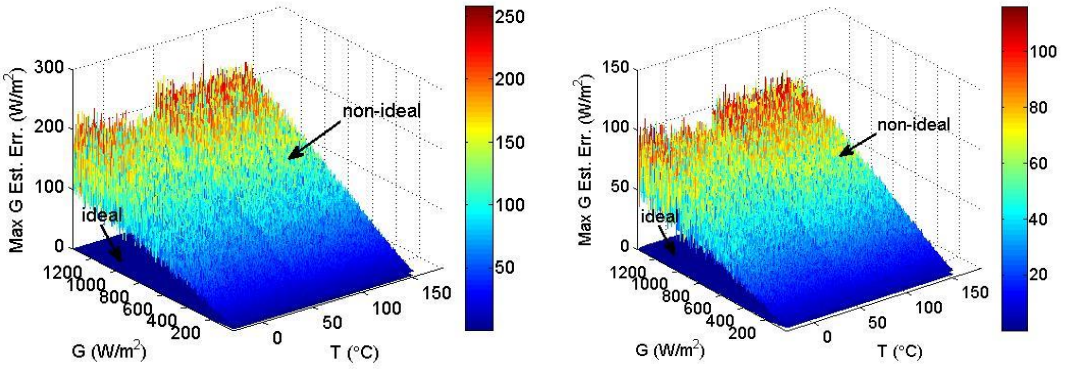

Fig. 4.9 Comparison of maximum solar insolation level estimation absolute error between ideal scenario and non-ideal scenario (left: 10-bit ADC, right: 12-bit ADC)

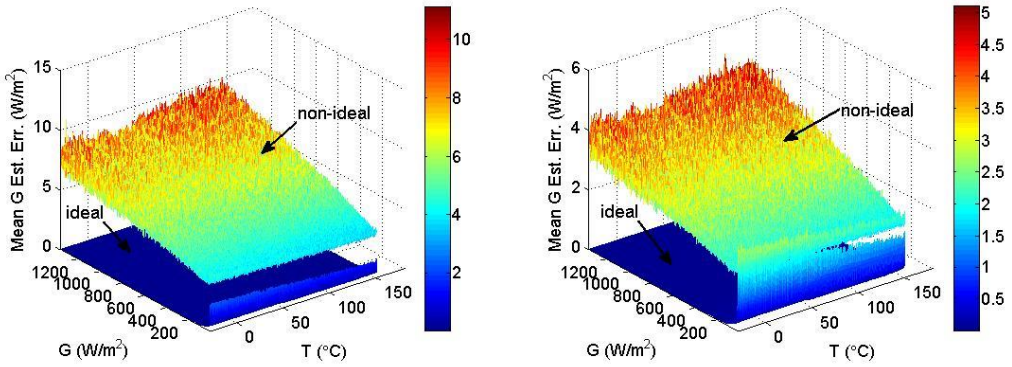

Fig. 4.10 Comparison of mean solar insolation level estimation absolute error between ideal scenario and non-ideal scenario (left: 10-bit ADC, right: 12-bit ADC)

Fig. 4.9 and Fig. 4.10 compare the maximum absolute error and mean absolute error for solar insolation level estimation between non-ideal and ideal scenario. From Fig. 4.9 and Fig. 4.10, it is observed that the measurement error has an influence on the solar insolation estimation. The maximum absolute solar insolation estimation error increases linearly as the PV solar insolation level increases. On average, the

estimation error in non-ideal scenario is higher and it varies from 4W/m^2 to 10W/m^2 and 2W/m^2 to 5W/m^2 for 10-bit ADC and 12-bit ADC respectively.

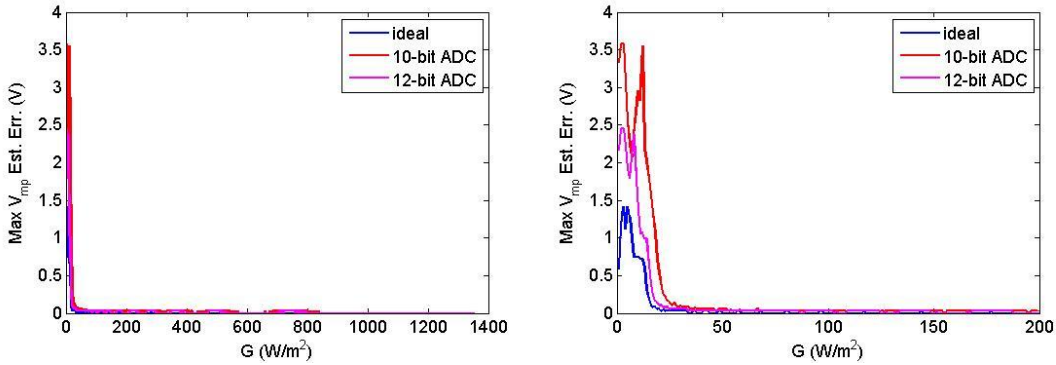

Fig. 4.11 Comparison of maximum V_{mp} estimation absolute error between non-ideal and ideal scenario at nominal temperature (left: full view; right: closer view, G < 200 W/m^2)

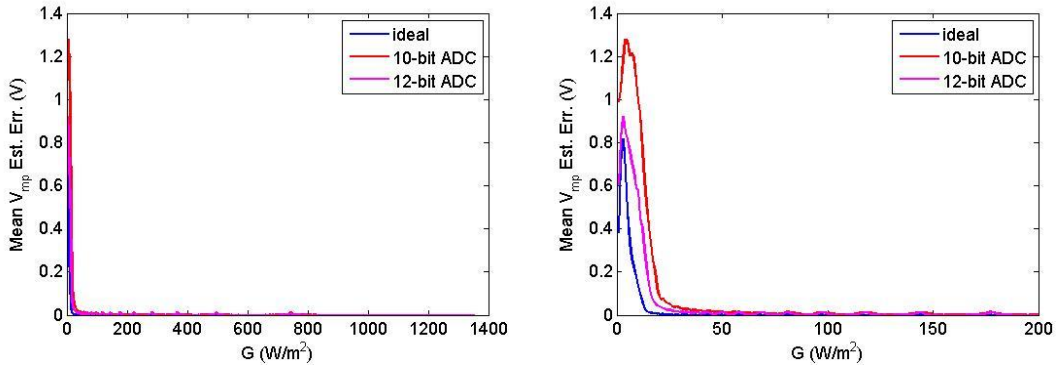

Fig. 4.12 Comparison of mean V_{mp} estimation absolute error between non-ideal and ideal scenario at nominal temperature (left: full view; right: closer view, G < 200 W/m^2)

Fig. 4.11 and Fig. 4.12 compare the maximum V_{mp} estimation absolute error and mean V_{mp} estimation absolute error between non-ideal scenario and ideal case at nominal temperature (T = 28°C). The V_{mp} estimation performance starts to deteriorate when the PV solar insolation is lesser than 100W/m^2 in the scenario when there is random measurement error. When the solar insolation is above 100W/m^2, the algorithm gives less than 0.05V V_{mp} estimation error. With the estimated MPP voltage, the tracking efficiency is calculated and its worst case is plotted in Fig. 4.13.

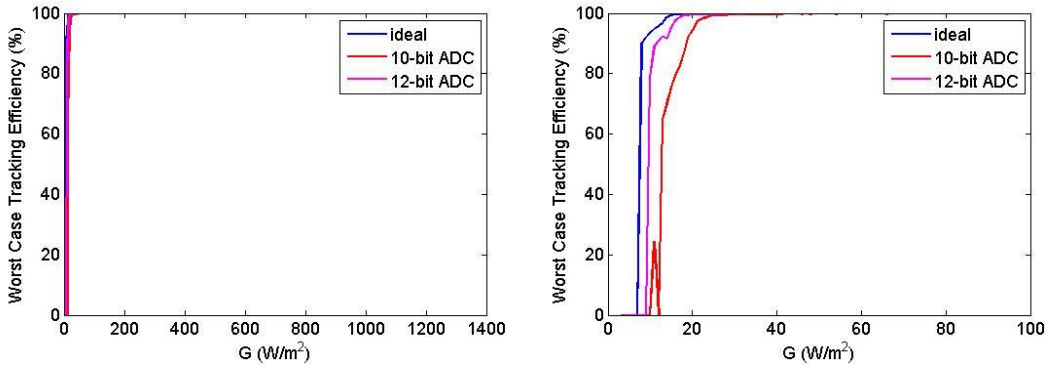

Fig. 4.13 Comparison of worst case tracking efficiency between non-ideal and ideal scenario at nominal temperature (left: full view; right: closer view, G < 100W/m^2)

Fig. 4.13 shows the worst case tracking efficiency between non-ideal and ideal scenario. From the comparison, the tracking performance of the SIMPPE algorithm is able to maintain above 99 % when the PV solar insolation is above 50 W/m^2 given the measurement error is within ± 3 LSB for 10-bit ADC. Therefore, it is concluded that the tracking performance of the SIMPPE algorithm is less sensitive towards measurement error.

4.3. **Simulation Study of SIMPPE Algorithm**

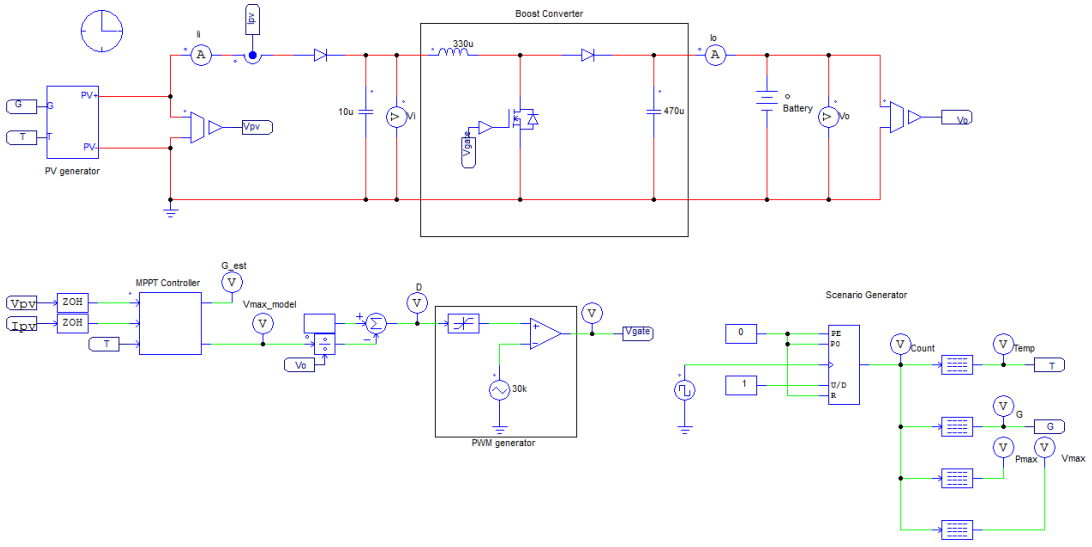

Fig. 4.14 PSIM-based simulation model of PV system with the SIMPPE algorithm

The SIMPPE algorithm has been implemented using PSIM-based simulation as shown in Fig. 4.14. The simulation study is to verify the SIMPPE algorithm in satellite operating scenarios and compare its performance with the conventional MPPT methods. To have fair comparison, the PV and boost converter parameters used are the same as in Chapter 3. Similarly, four different satellite scenarios in Fig. 3.3 are used. The proposed algorithm in Algorithm 4.1 have been implemented for the MPPT controller in the simulation. The simulation results for the satellite under normal operating mode and safe-hold operating mode are presented in Fig. 4.15 and Fig. 4.16.

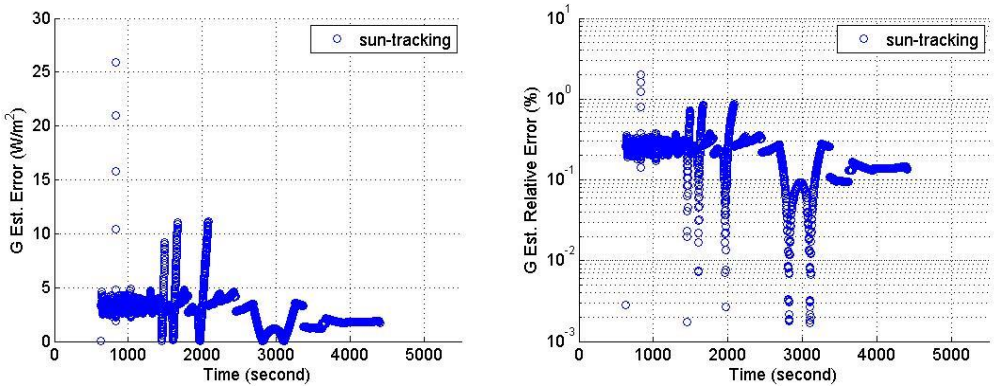

(a) normal operating mode with sun-tracking

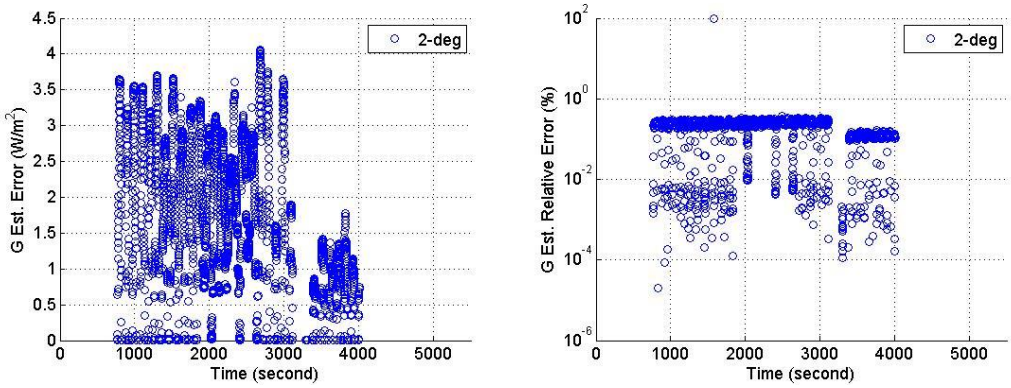

(b) safe-hold operating mode with 2 degrees/s rotation

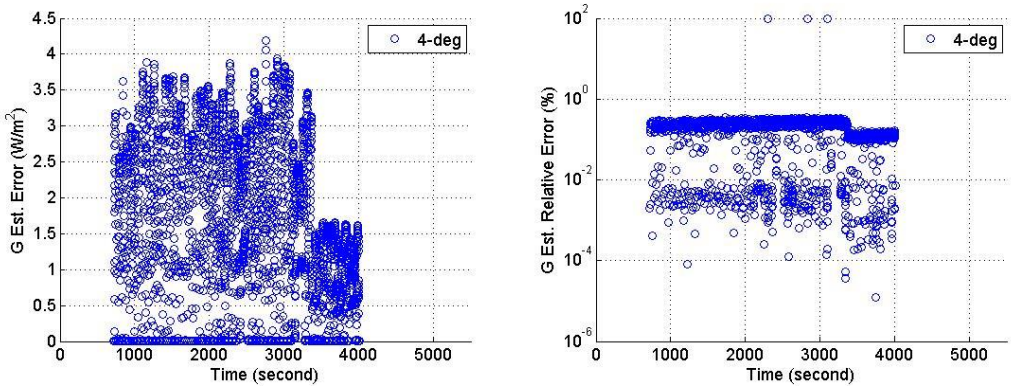

(c) safe-hold operating mode with 4 degrees/s rotation

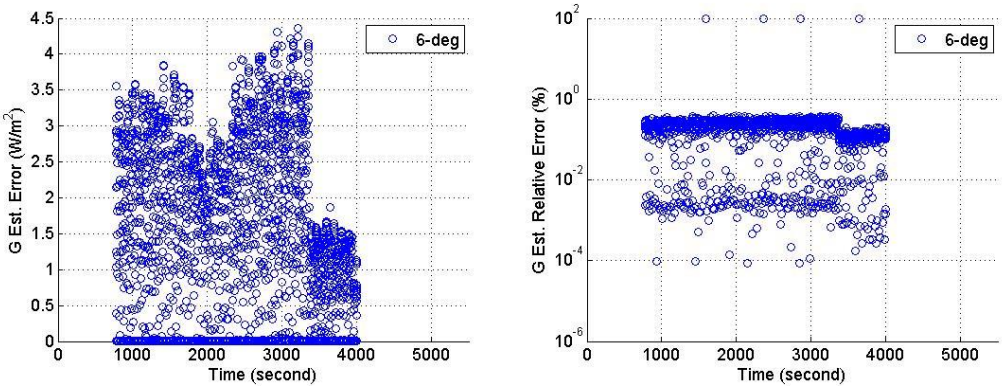

(d) safe-hold operating mode with 6 degrees/s rotation

Fig. 4.15 Solar insolation estimation absolute error (left) and relative error (right) under different scenarios

The simulation results in Fig. 4.15 show that the SIMPPE algorithm is able to give a good estimation of solar insolation level. Its maximum error is less than 30W/m^2. For normal operating scenario, the solar insolation relative estimation error maintains below 5% at all time. For safe-hold operating scenario, there is a sudden spike in the relative estimation error and it goes to 100%. This is due to the PV experiencing low solar insolation level which is below 200W/m^2. Table 4.4 summarizes the error of the solar insolation level estimation, G_{est}.

Table 4.4 Solar insolation level estimation error under different satellite operating scenarios

	Sun tracking	2 degree/s rotation	4 degree/s rotation	6 degree/s rotation
Maximum absolute error	25.9527 W/m^2	4.0594 W/m^2	4.1904 W/m^2	4.3586 W/m^2
Mean absolute error	2.6997 W/m^2	1.7086 W/m^2	1.6806 W/m^2	1.7422 W/m^2

From Table 4.4, it is observed that the SIMPPE algorithm provides an accurate estimation of solar insolation level during normal and safe-hold operating mode. With

the estimated solar insolation level, V_{mp} under different satellite scenarios is estimated by solving *I-V* equation using the Newton-Raphson method and plotted in Fig. 4.16.

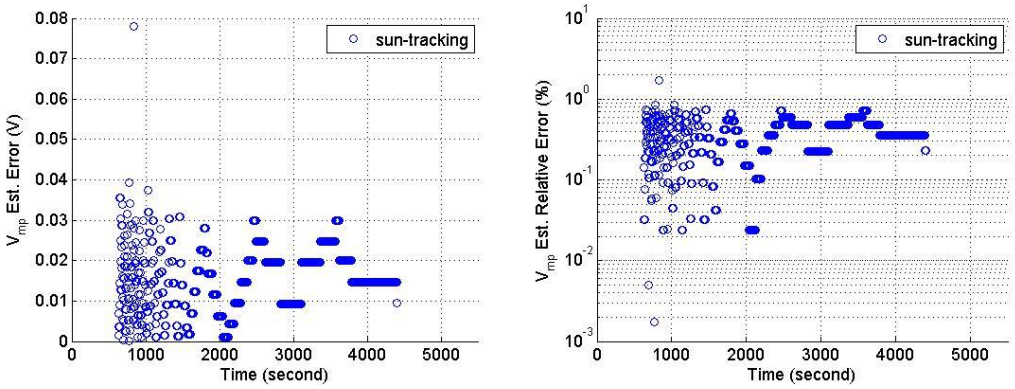

(a) normal operating mode with sun-tracking

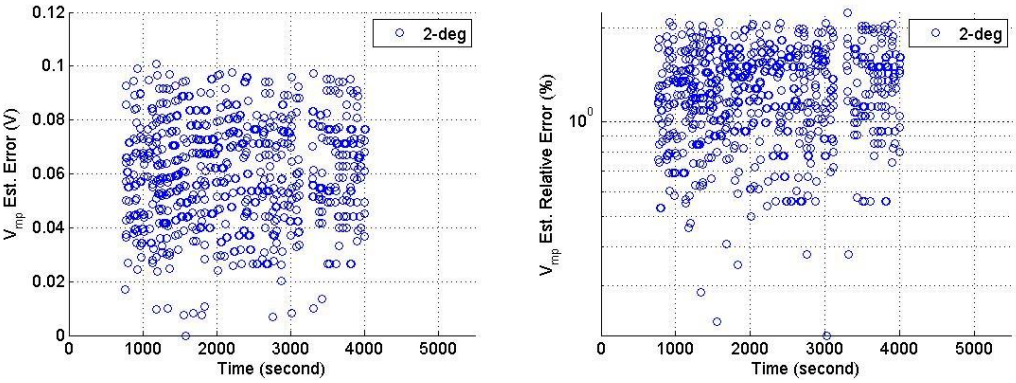

(b) safe-hold operating mode with 2 degrees/s rotation

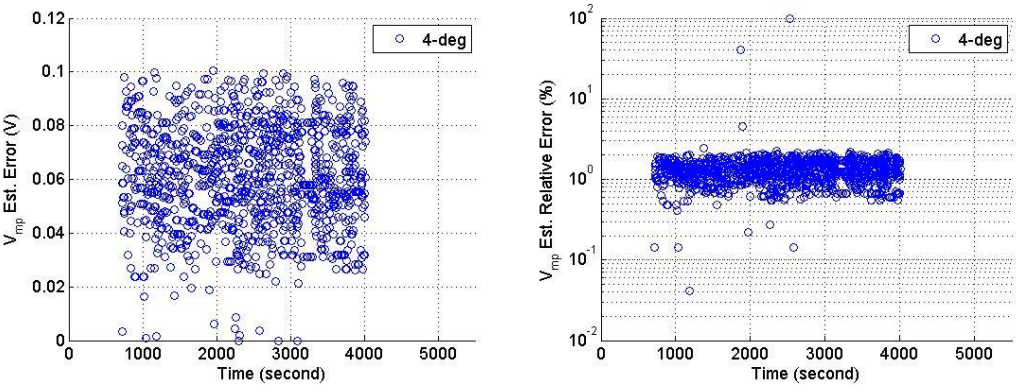

(c) safe-hold operating mode with 4 degrees/s rotation

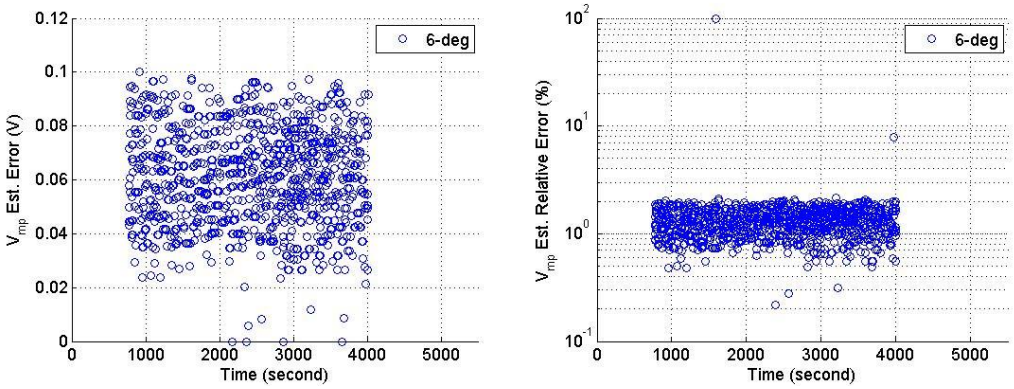

(d) safe-hold operating mode with 6 degrees/s rotation

Fig. 4.16 V_{mp} estimation absolute error (left) and relative error (right) under different scenarios

Fig. 4.16 shows the V_{mp} estimation error under different satellite operating scenarios. From Fig. 4.16, it is noticed that the V_{mp} estimation error is less than 0.1V in all satellite operating scenarios. Moreover, the V_{mp} estimation relative error maintain below 2% at most of the time. This shows that the SIMPPE algorithm is able to track the MPP of the PV under different satellite operating scenarios. From the simulation result, the tracking efficiency is calculated using (3.1) and illustrated in Table 4.5.

Table 4.5 Comparison of tracking efficiency under different satellite operation scenarios

	Sun tracking	2 degree/s rotation	4 degree/s rotation	6 degree/s rotation
SIMPPE	99.80%	98.29 %	98.17 %	98.07 %
P&O (best case)	99.64% (ΔD = 1%)	92.28% (ΔD = 3%)	85.64% (ΔD = 4%)	93.11% (ΔD = 1%)
InC (best case)	99.64% (ΔD = 1%)	92.34% (ΔD = 3%)	85.56% (ΔD = 4%)	93.15% (ΔD = 1%)

Table 4.5 summarizes the tracking efficiency of the SIMPPE algorithm under four different satellite scenarios. From the table, it is noted that the tracking efficiency of the SIMPPE algorithm reduces when the satellite is rotating faster. This is due to the

limitation of the SIMPPE algorithm in the low solar insolation level situation. As the satellite rotates faster, the frequent the satellite experiences low solar insolation level. Nevertheless, the SIMPPE algorithm gives a better tracking efficiency than the conventional MPPT methods in all satellite operating scenarios.

4.4. **Experimental Validation of SIMPPE Algorithm**

In previous section, it is observed that the measurement errors will affect the tracking performance of the SIMPPE algorithm in software simulation. Thus, a hardware-in-the-loop test system is setup to validate the SIMPPE algorithm using real sensing circuit instead of software simulation.

This section presents the experimental results to validate the SIMPPE algorithm. A hardware-in-the-loop test system using solar array simulators and electronic loads has been setup to achieve space scenarios in laboratory environment. The overall test setup is developed based on a virtual instrumentation concept. By using LabVIEW, the solar array simulator and electronic load are controlled using General Purpose Interface Bus (GPIB) commands as shown in Fig. 4.17.

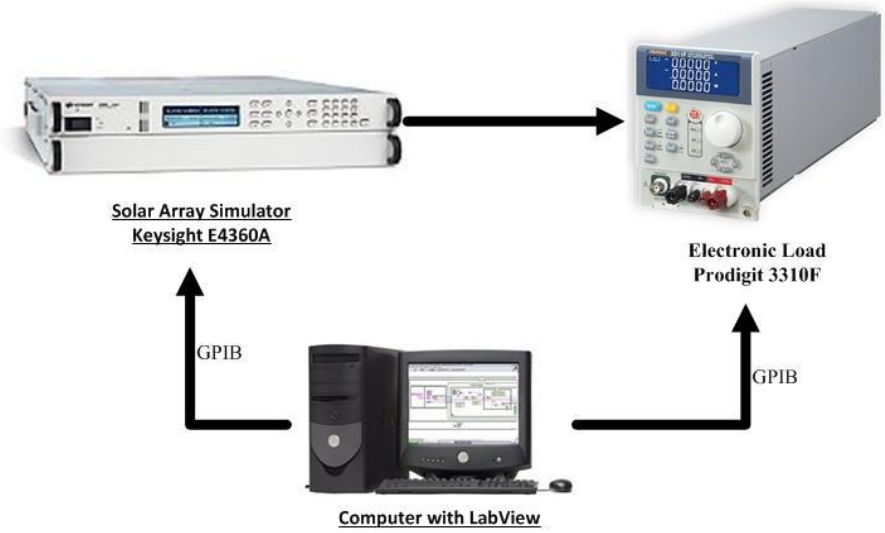

Fig. 4.17 Hardware-in-the-loop experimental test setup

The solar array simulator is used to emulate the actual PV arrays output based on temperature and solar insolation. The SIMPPE algorithm has been programmed in LabVIEW and the voltage and current measurements will be provided by electronic load via GPIB commands. Each time the algorithm takes a measurement, the MPP voltage is computed using the Newton-Raphson method and used to set the load voltage of the electronic load.

To validate the SIMPPE algorithm experimentally, the simulation results in Section 4.3 were compared with results obtained through experiments conducted using hardware-in-the-loop setup in Fig. 4.17. Four sets of PV array temperature and solar insolation profile in Fig. 3.3 are programmed into solar array simulator to simulate different satellite operating scenarios. The comparison between simulation and experimental results are presented in Fig. 4.18.

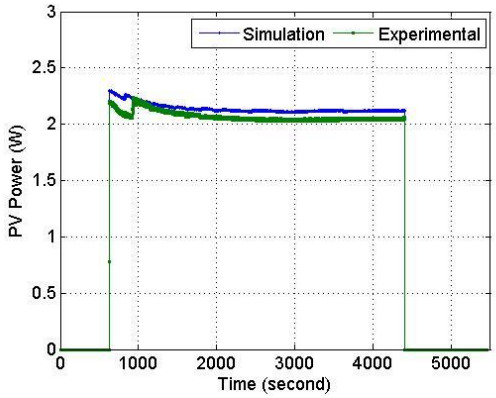

(a) normal operating mode with sun-tracking

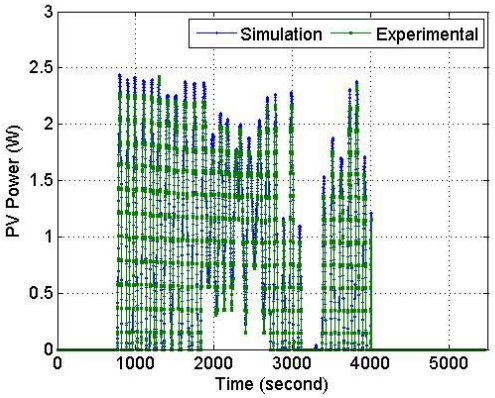

(b) safe-hold operating mode with 2 degrees/s rotation

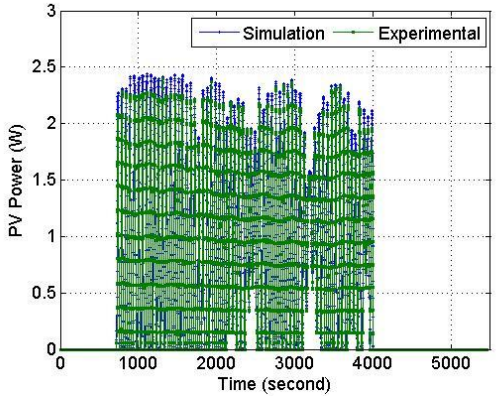

(c) safe-hold operating mode with 4 degrees/s rotation

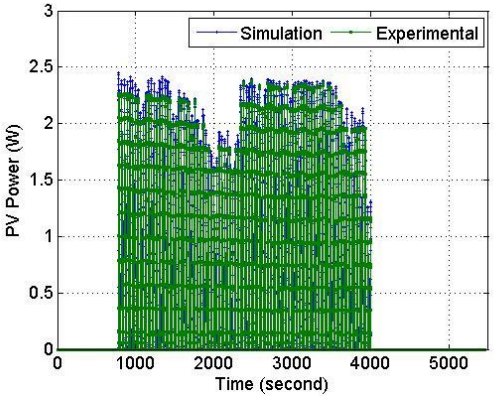

(d) safe-hold operating mode with 6 degrees/s rotation

Fig. 4.18 Experimental tracked power vs simulation tracked power for SIMPPE algorithms under different scenarios

From Fig. 4.18, it is observed that the experimental results match with the simulation results. In all satellite operating scenarios, the difference of simulation and experimental results is less than 0.2W at most of the time. The tracking efficiency of experimental are calculated and compared with simulation result in Table 4.6.

Table 4.6 Tracking efficiency comparison for the SIMPPE algorithm

	sun tracking	2 degree/s rotation	4 degree/s rotation	6 degree/s rotation
Simulation	99.80%	98.29 %	98.17 %	98.07 %
Experimental	96.56%	91.27%	91.43%	91.58%

Thus, the tracking performance of the SIMPPE algorithm have been validated.

4.5. **Summary**

The feasibility of the SIMPPE algorithm has been investigated under different temperature and solar insolation level scenarios that range from -30°C to 150°C and 1W/m^2 to 1353W/m^2. From the result, it shows that the maximum solar insolation estimation error is less than 3W/m^2 for varying PV operating point under different temperatures and solar insolation level scenarios. With the estimated solar insolation level, the SIMPPE algorithm is able to give an accurate estimation of V_{mp} with its maximum absolute estimation error is less than 0.05V at 95% of temperature and solar insolation level scenarios. The drawback of the SIMPPE algorithm is its poorer performance in low solar insolation level scenarios. However, the PV maximum power is low and negligible during low solar insolation level. Under the condition of measurement affected by ADC resolution, the solar insolation level estimation performance will be affected while the tracking performance is still able to give 95% tracking efficiency for solar insolation level above 50W/m^2.

The SIMPPE algorithm has been implemented in PSIM-based simulation with different satellite operating scenarios. The simulation results show that the tracking efficiency of the SIMPPE algorithm has improved between 0.16% and 8.42%

comparing to best case of P&O and InC. Moreover, the SIMPPE algorithm also has the advantage of zero steady-state oscillation at MPP while the conventional MPPT methods encountered steady-state oscillation. The solar array simulator and electronic load are integrated with LabVIEW software to form the hardware-in-the-loop test system. The test system is used to validate the SIMPPE algorithm experimentally. Experimental results show that the tracking efficiency for the SIMPPE algorithm under normal operating and safe-hold operating scenarios are 96% and 91% respectively.

CHAPTER 5. TEMPERATURE AND MAXIMUM POWER POINT ESTIMATION (TMPPE)

The SIMPPE algorithm presented in Chapter 4 required temperature sensor to estimate maximum power point (MPP) as compare to the conventional maximum power point tracking (MPPT) method. In this chapter, an improvement has been made such that the model based MPPT is able to estimate both photovoltaic (PV) temperature and solar insolation level.

Using multiple pairs of PV measurement and single diode PV model, the estimation of temperature is formulated with the knowledge of voltage and current measured from the PV array. The temperature and MPP estimation (TMPPE) algorithm estimates the MPP with the estimated temperature and solar insolation level. The feasibility of TMPPE algorithm has been studied through simulation study. The simulation study has been conducted under different environmental conditions and different levels of random noise to analyse its feasibility. The performance of the TMPPE algorithm will be verified using the same PSIM-based simulation and operation scenarios from Chapter 3. Finally, the TMPPE algorithm is validated experimentally using the hardware-in-the-loop test system in Chapter 4.

5.1. **TMPPE Algorithm**

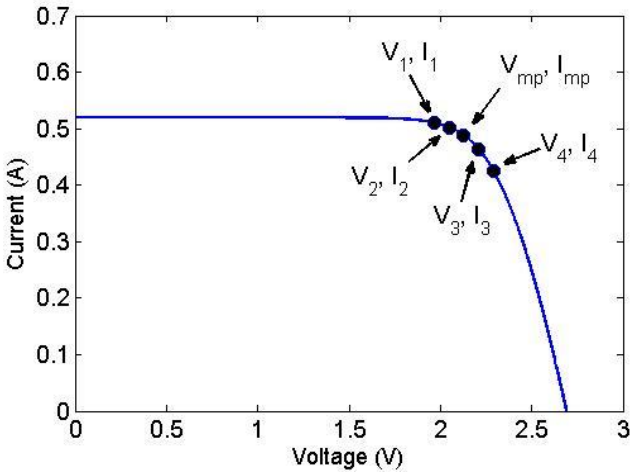

Fig. 5.1 Points used by the TMPPE algorithm

The TMPPE algorithm solves the single diode model with the measurements of four pairs of voltage and current point ((V_1, I_1), (V_2, I_2), (V_3, I_3) & (V_4, I_4)) as shown in Fig. 5.1. The required condition for these points is that they must be taken in same environmental condition and they are close to MPP. This is because when the operating point is close to MPP, the $\frac{dI_{PV}}{dV_{PV}}$ is significant to estimate PV temperature.

The TMPPE algorithm is able to solve for the temperature information by estimate solar insolation level ($G_{est,1}$, $G_{est,2}$, $G_{est,3}$, $G_{est,4}$). The solar insolation level estimation equation in (4.8) can be rewritten for different temperature, T as follows:

$$G_{est,k}(T) = \frac{\tilde{I}_k + \frac{I_{sc,n} + K_i \Delta T}{\exp\left(\frac{V_{oc,n} + K_v \Delta T}{a(T) N_s V_t(T)}\right) - 1}\left[\exp\left(\frac{\tilde{V}_k + R_s(T)\tilde{I}_k}{a(T) N_s V_t(T)}\right) - 1\right] + \frac{\tilde{V}_k + R_s(T)\tilde{I}_k}{R_p(T)}}{\frac{R_p(T) + R_s(T)}{R_p(T)} I_{sc,n} + K_i \Delta T} \times G_n \quad (5.1)$$

Given that the environmental condition is constant for these points taken, the estimated solar insolation level should be close to each other therefore their difference are close to zero.

$$\Delta G_{est}(T) = \left|G_{est,1}(T) - G_{est,2}(T)\right| + \left|G_{est,2}(T) - G_{est,3}(T)\right| + \left|G_{est,3}(T) - G_{est,4}(T)\right| \quad (5.2)$$

With G_{est}, T_{est}, a, R_s, and R_p, the *I-V* curve can be reconstructed and the MPP can be estimated by solving $I = f(V, I)$. The transcendental equation, $I = f(V, I)$ can be solved by numerical methods such as Newton-Raphson method.

An overview of the TMPPE algorithm is shown in Algorithm 5.1.

Step 1: Measure PV voltage and current at different operating point

$$\tilde{V}_1, \tilde{I}_1, \tilde{V}_2, \tilde{I}_2, \tilde{V}_3, \tilde{I}_3, \tilde{V}_4, \tilde{I}_4$$

Step 2: Initialize a, R_s and R_p from lookup table for different temperature, -30 °C ≤ T ≤ 150 °C

Step 3: Recursively solve G_{est} for different set of a, R_s and R_p for different temperature, -30 °C ≤ T ≤ 150 °C

$$G_{est,1}, G_{est,2}, G_{est,3}, G_{est,4}$$

Step 4: Obtain absolute difference of G_{est} to determine the correct temperature by finding minimum of ΔG_{est}

$$\Delta G_{est}(T) = \left|G_{est,1}(T) - G_{est,2}(T)\right| + \left|G_{est,2}(T) - G_{est,3}(T)\right| + \left|G_{est,3}(T) - G_{est,4}(T)\right|$$

Step 5: With T_{est} and G_{est}, recursively solve the following equation $I = f(V, I)$, for $0 \le V \le V_{oc}$

$$I = I_{ph} - I_{rs}\left[\exp\left(\frac{V + R_s I}{aN_s V_t}\right) - 1\right] - \frac{V + R_s I}{R_p}$$

Step 6: Find V_{mp} by calculate P for $0 \le V \le V_{oc}$

Algorithm 5.1 Proposed TMPPE algorithm

5.2. **Feasibility Studies of TMPPE Algorithm**

Based on the proposed approach, the feasibility of the TMPPE algorithm is first investigated. A simulation study has been conducted using MATLAB. For the simulation study, the PV parameters is configured based on Azur Space solar cell and its specification is shown in Table 4.1. Considering boost topology used in Fig. 3.1 and the battery parameters in Table 3.1, the voltage step is set to 100mV for the four pairs of measurements to meet the allowed input voltage range in practical boost converter. The simulation has been conducted on different temperatures (T = -22°C, 28°C, 78°C) and solar insolation levels (G = 400W/m^2, 800W/m^2, 1353W/m^2). With the four pairs of measurements, the temperature is estimated using the TMPPE algorithm in Algorithm 5.1 and the results are shown in Fig. 5.2.

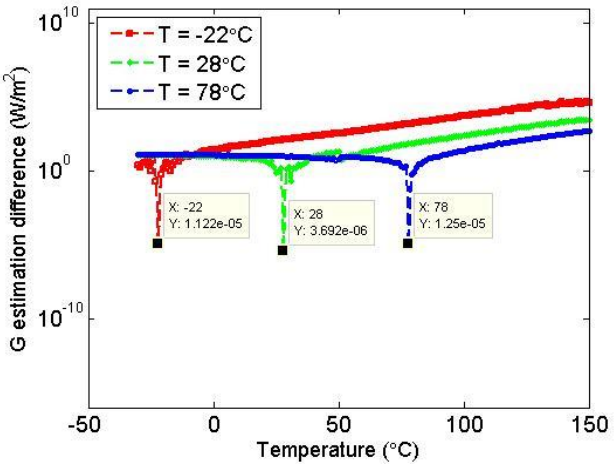

(a) G = 400W/m^2

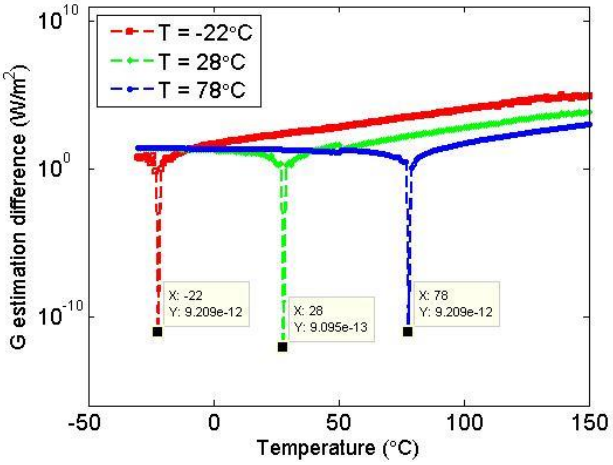

(b) G = 800W/m^2

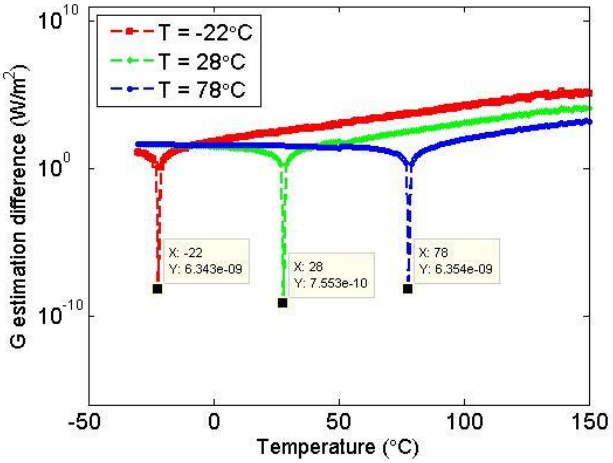

(c) G = 1353W/m^2

Fig. 5.2 Temperature estimation under different temperature and solar insolation level

Fig. 5.2 shows that the correct temperature will give lowest ΔG_{est}. The solar insolation level can be estimated using (5.1) with the accurate estimated temperature. With the estimated temperature and solar insolation level, the *I-V* curve can be reconstructed and the MPP can be solved using the Newton-Raphson method.

As shown in Fig. 5.2, the TMPPE algorithm is able to find the correct temperature using (5.1) and (5.2) in ideal scenario. As mentioned in Chapter 4, the drawback of the model based MPPT algorithm is the sensing errors. Simulation has been extended to

study the effect of measurement error towards temperature and solar insolation level estimation.

In this simulation study, different range of measurement error has been set to investigate the feasibility of the TMPPE algorithm. The temperature and solar insolation level of PV are set at nominal condition (T = 28°C, G = 1353W/m^2). The range of measurement error is set between 0.1% and 1% in step of 0.1% of the voltage and current measurement range. The voltage and current measurement range is set to 6V and 1A respectively to cover all the PV measurements under any environmental condition. In the Monte Carlo simulation test, 1000 simulations have been conducted for each range of measurement error. The statistical mean of the temperature and solar insolation level estimation results are calculated and plotted in Fig. 5.3 and Fig. 5.4.

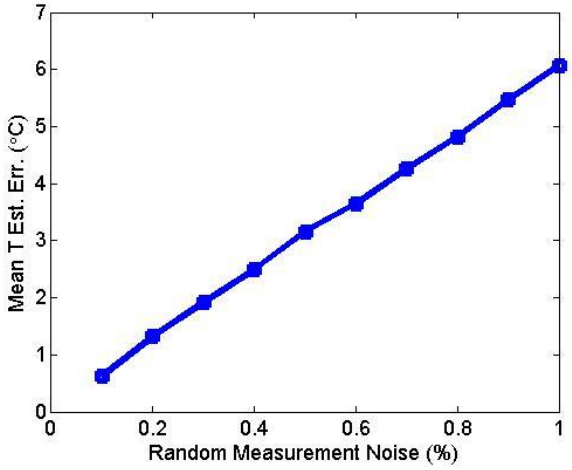

Fig. 5.3 Absolute mean error of temperature estimation under different measurement noise levels

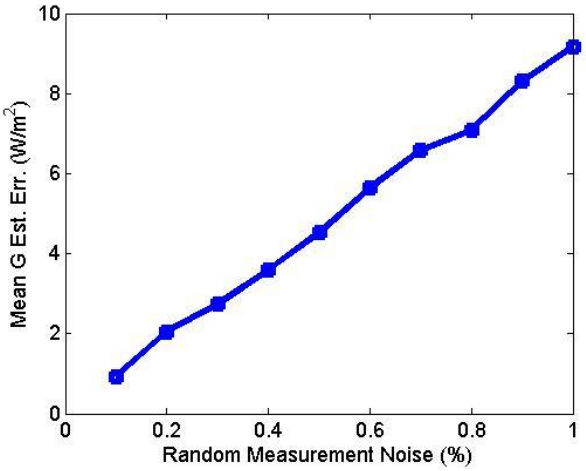

Fig. 5.4 Absolute mean error of solar insolation level estimation under different measurement noise levels

From Fig. 5.3 and Fig. 5.4, it is observed that the temperature and solar insolation level estimations are linearly affected by the measurement noise level. As the measurement noise increases from 0.1% to 1.0%, the mean of temperature estimation error increases from 0.622°C to 6.06°C while the mean of solar insolation level estimation error increases from 0.925W/m^2 to 9.1537W/m^2.

With the estimated temperature and solar insolation level, the *I-V* curve can be reconstructed by solving (4.1) using the Newton-Raphson method. Thus, V_{mp} can be estimated through the reconstructed *I-V* curve and its power loss will be evaluated.

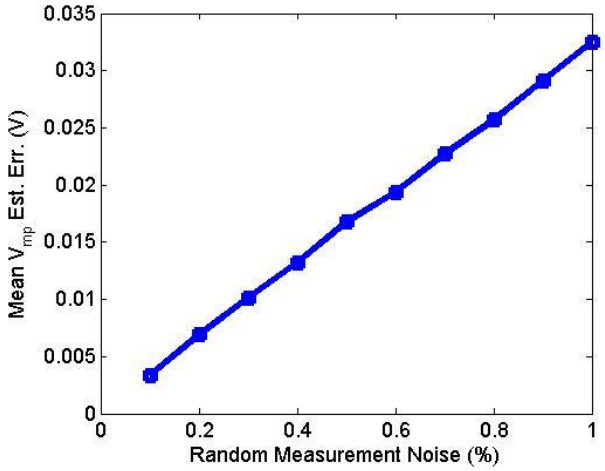

Fig. 5.5 Mean MPP voltage estimation error under different measurement noise levels

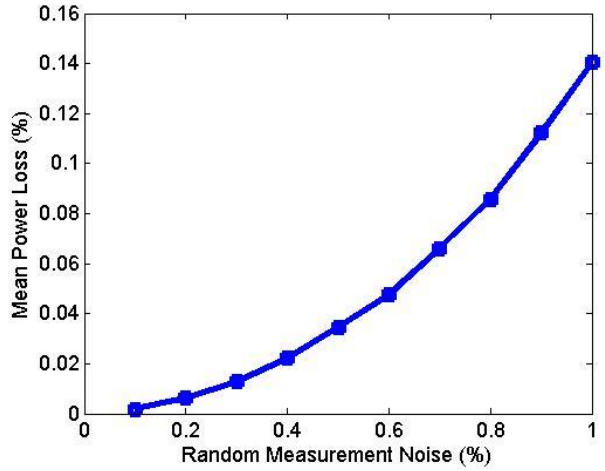

Fig. 5.6 Mean power loss under different measurement noise levels

Fig. 5.5 and Fig. 5.6 show the effect of different measurement noise levels on MPP voltage estimation and power loss. In all measurement noise scenarios, the proposed method gives less than 1% V_{mp} estimation error and its tracking efficiency is above 98%. This show that the tracking performance of the TMPPE algorithm is not sensitive to measurement noise.

The mean (μ) and standard deviation (σ) for simulation are calculated to evaluate the performance of SIMPPE algorithm at 3-sigma (μ + 3σ). The absolute error for

temperature, solar insolation level and maximum power point voltage estimation at 3-sigma are summarized in Table 5.1.

Table 5.1 Summary of estimation error at 3-sigma (T = 28°C, G = 1353W/m^2)

Measurement error	T estimation absolute error (°C) at 3-sigma	G estimation absolute error (W/m^2) at 3-sigma	V_{mp} estimation absolute error (V) at 3-sigma	Average power loss (%) at 3-sigma
0.1% (± 6mV / ± 1mA)	2.2020	3.0292	0.0120	0.0018
0.2% (± 12mV / ± 2mA)	4.0109	6.3530	0.0212	0.0257
0.3% (± 18mV / ± 3mA)	5.4687	8.7878	0.0291	0.0520
0.4% (± 24mV / ± 4mA)	7.1931	11.4405	0.0385	0.0935
0.5% (± 30mV / ± 5mA)	8.7500	14.0491	0.0469	0.1402
0.6% (± 36mV / ± 6mA)	10.4125	18.2224	0.0558	0.1968
0.7% (± 42mV / ± 7mA)	12.2139	21.4428	0.0654	0.2823
0.8% (± 48mV / ± 8mA)	14.0138	23.3487	0.0749	0.3743
0.9% (± 54mV / ± 9mA)	15.7473	26.7091	0.0842	0.4997
1.0% (± 60mV / ± 10mA)	17.5391	29.8485	0.0950	0.6501

Next, we evaluate the feasibility of the TMPPE algorithm under different temperature and solar insolation level conditions. In the simulation, 0.5% random measurement noise is selected to cover the accuracy of 10-bit and 12-bit ADC in Table 4.3. The simulation studies have been conducted with temperature ranging from -20°C to 140°C in step of 10°C and solar insolation level ranging from 200W/m^2 to 1200W/m^2 in step of 100W/m^2. In the Monte Carlo simulation, the simulation has been conducted 1000 times for each combination of temperature and solar insolation level. The mean (μ) and standard deviation (σ) are calculated to evaluate the feasibility

of the TMPPE algorithm at 3-sigma ($\mu + 3\sigma$). The estimation results and power loss are plotted in Fig. 5.7-Fig. 5.10.

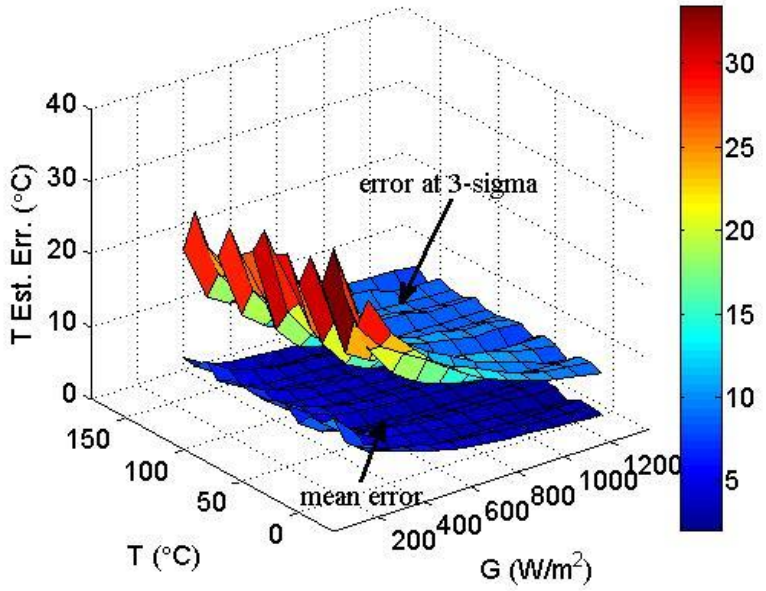

Fig. 5.7 Temperature estimation performance under different environmental conditions

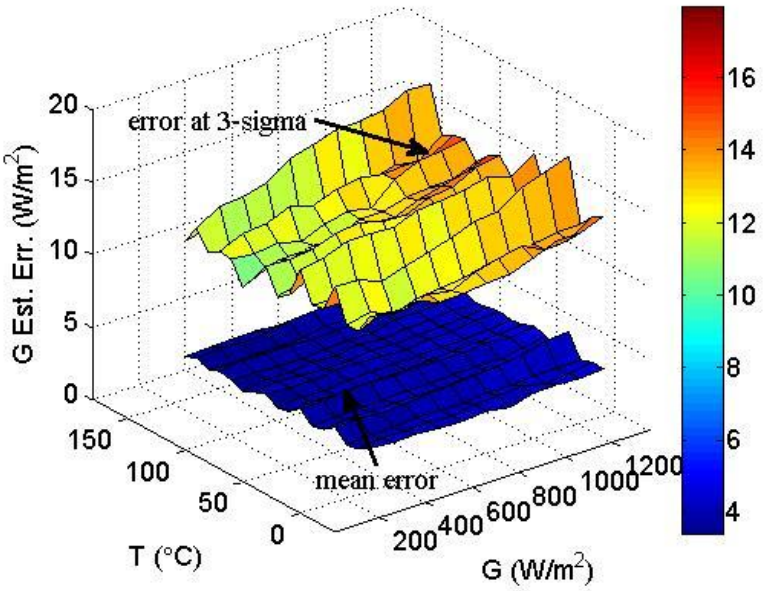

Fig. 5.8 Solar insolation level estimation performance under different environmental conditions

From Fig. 5.7, it is observed that the mean absolute error of temperature estimation is less than 10°C in all cases. Fig. 5.7 shows that absolute error of temperature estimation is affected by solar insolation level. The temperature estimation absolute error at 3-sigma is less than 15°C when solar insolation level is above 600W/m^2 and it shoots up to 35°C when solar insolation level is 200W/m^2. On the other hand, the solar insolation level estimation error is less sensitive to environmental condition. As shown in Fig. 5.8, the mean absolute error is below 6W/m^2 in all cases and the error at 3-sigma is between 10W/m^2 to 18W/m^2. A closer examination at Fig. 5.8 reveals that solar insolation level estimation error increases slightly with an increase in solar insolation level.

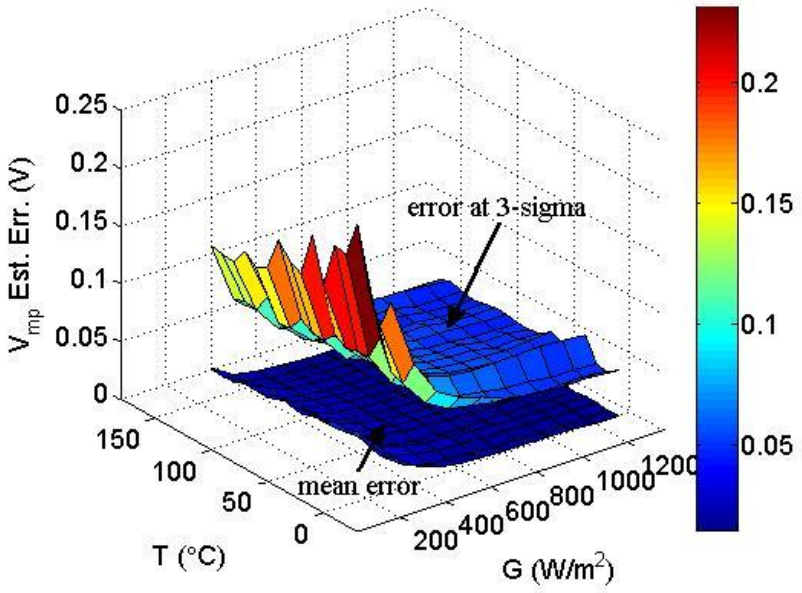

Fig. 5.9 V_{mp} estimation performance under different environmental conditions

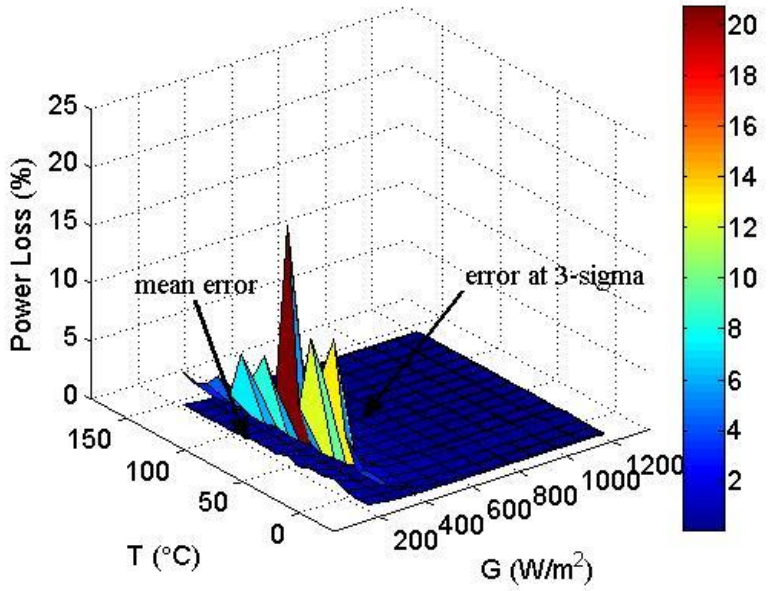

Fig. 5.10 Power loss under different environmental conditions

Fig. 5.9 and Fig. 5.10 show the performance of the TMPPE algorithm in estimating MPP voltage and its power loss. Similar to the temperature estimation, the MPP voltage estimation deteriorates when the solar insolation level is below 600W/m^2. Nevertheless, the power loss at 3-sigma increases from 0.61% to 20.67% when solar insolation level decreases from 400W/m^2 to 200W/m^2. Thus, it is recommended to execute the algorithm when solar insolation level is above 400W/m^2.

5.3. **Simulation Study of TMPPE Algorithm**

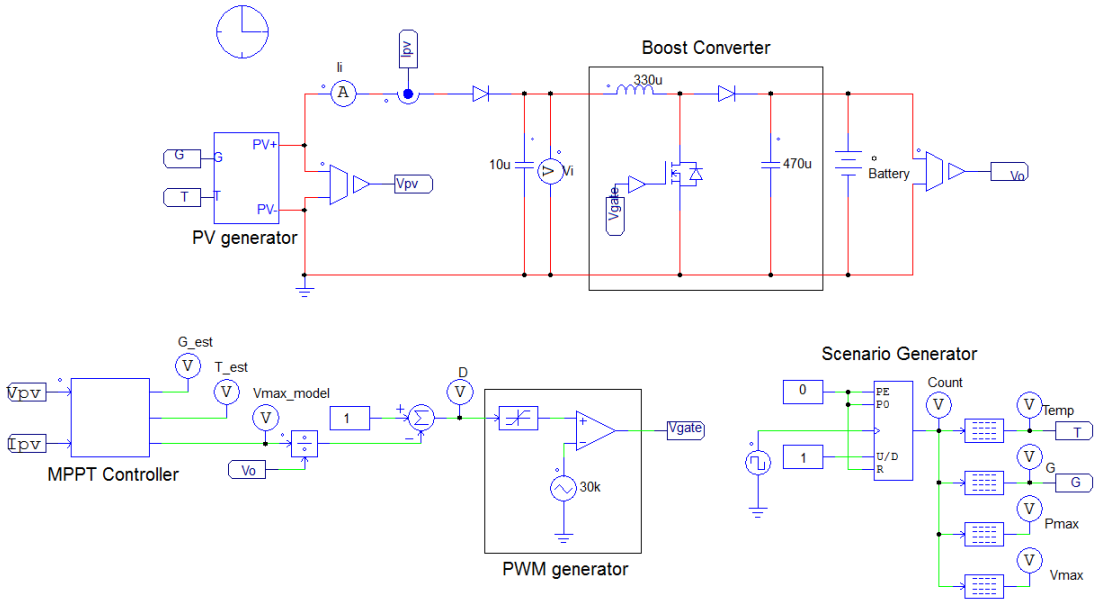

Fig. 5.11 PSIM-based simulation model of PV system with the TMPPE algorithm

The TMPPE algorithm has been implemented using PSIM-based simulation as shown in Fig. 5.11. The simulation study is to verify the TMPPE algorithm in satellite scenarios and compare its performance with the conventional MPPT methods and the SIMPPE algorithm. The PV and boost converter parameters in Chapter 3 are used in this study. Four sets of PV array temperature and solar insolation level profile in Fig. 3.3 are used to simulate different satellite operating scenarios. The TMPPE algorithm in Algorithm 5.1 have been implemented for the MPPT controller in the simulation.

For practical implementation, certain conditions must be met to guarantee consistent temperature and solar insolation level estimation so that the MPP computation will be accurate. Due to the *I-V* characteristic of a PV array, the measurements must always fulfil the following conditions:

$$V_1 < V_2 < V_3 < V_4 \tag{5.3}$$

$$I_1 > I_2 > I_3 > I_4 \tag{5.4}$$

$$\frac{V_2 - V_1}{I_2 - I_1} < \frac{V_4 - V_3}{I_4 - I_3} \tag{5.5}$$

If any above conditions (5.3)-(5.5) not fulfilled, the TMPPE algorithm will not execute estimation and acquiring process is repeated until valid points is obtained. The estimation only valid if the following conditions are fulfilled:

$$400 > G_{est} > 1353 \tag{5.6}$$

$$\Delta G_{est}(T) < 100 \tag{5.7}$$

As previous study has shown, the TMPPE algorithm has poor performance when solar insolation level is below 400W/m^2. Thus, condition (5.6) filter any low solar insolation level scenario. Condition (5.7) is used to filter sudden solar insolation level change during acquisition.

The simulation results for the satellite under normal operating mode and safe-hold operating mode are presented in Fig. 5.12 and Fig. 5.13.

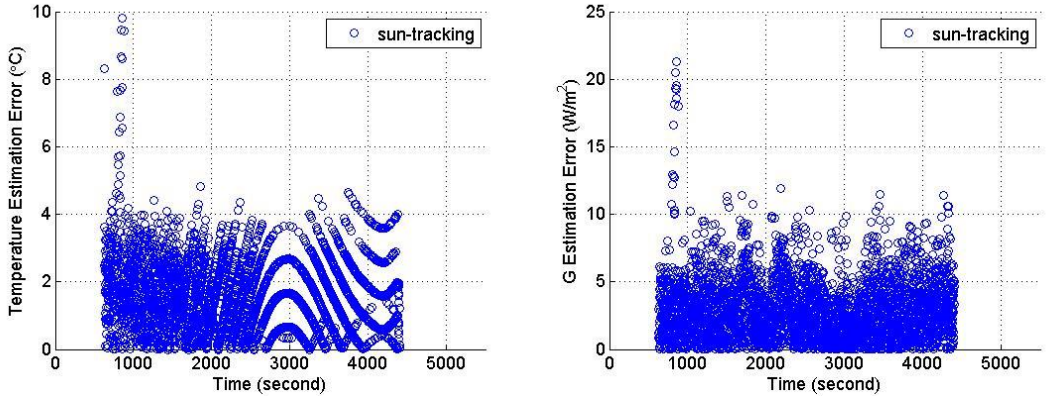

(a) Normal operating mode with sun-tracking

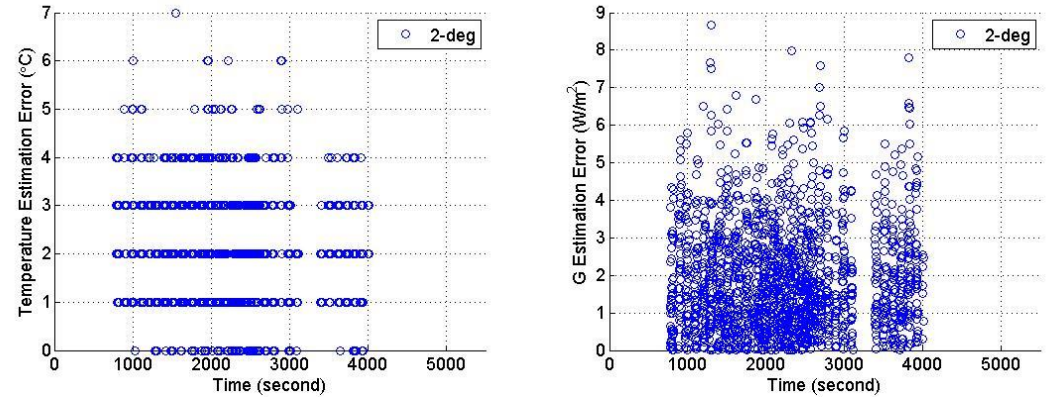

(b) Safe-hold operating mode with 2 degrees/s rotation

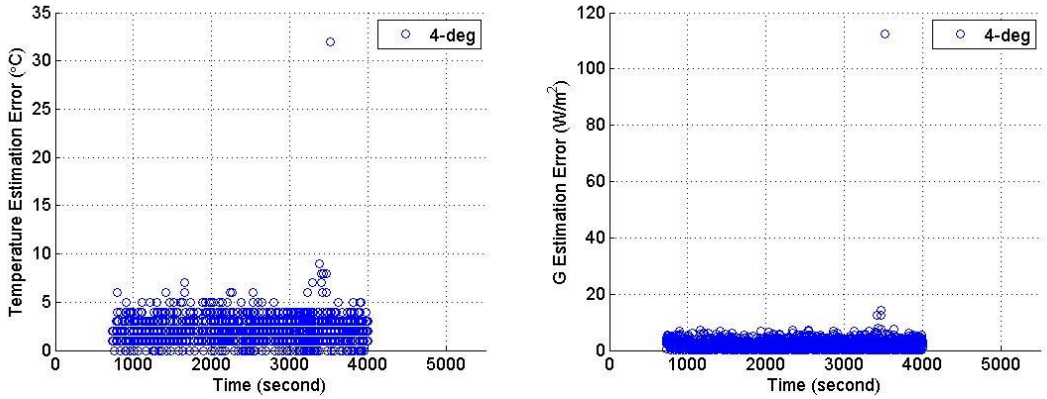

(c) Safe-hold operating mode with 4 degrees/s rotation

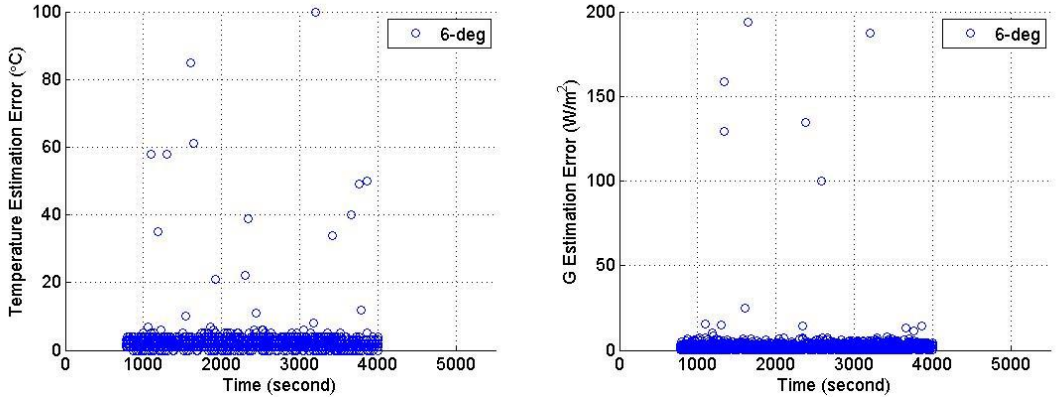

(d) Safe-hold operating mode with 6 degrees/s rotation

Fig. 5.12 Temperature and solar insolation level estimation absolute error under different scenarios

Fig. 5.12 shows the temperature and solar insolation level estimation error under different satellite operating scenarios. From Fig. 5.12, the TMPPE algorithm maintains both temperature and solar insolation level estimation error in term of less than 10°C

and 10W/m^2 respectively at most of the time. However, a closer examination reveals that sudden spike of the estimation error is happened when the PV solar insolation level is between 400W/m^2 to 600W/m^2.

With the estimated PV temperature and solar insolation level, V_{mp} under different satellite operation scenarios is estimated using Newton-Raphson method and its estimation error is plotted in Fig. 5.13.

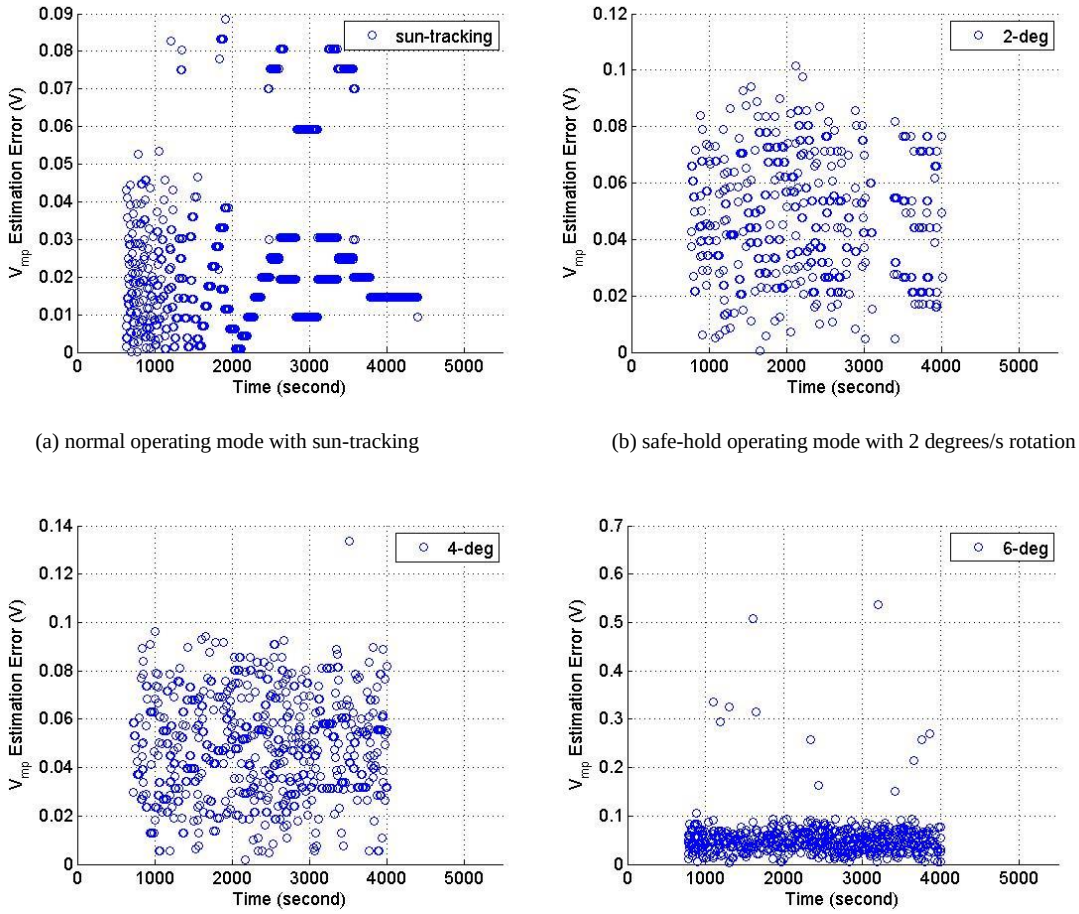

(a) normal operating mode with sun-tracking

(b) safe-hold operating mode with 2 degrees/s rotation

(c) safe-hold operating mode with 4 degrees/s rotation

(d) safe-hold operating mode with 6 degrees/s rotation

Fig. 5.13 MPP voltage estimation absolute error under different scenarios

Fig. 5.13 shows the V_{mp} estimation error for satellite normal operating mode and safe-hold operating mode. It is observed that V_{mp} estimation error is less than 0.1V at most of the time. Table 5.2 summarizes the mean absolute error for temperature

estimation, solar insolation level estimation and MPP voltage estimation under different satellite operating scenarios.

Table 5.2 Comparison of mean absolute error under different satellite operating scenarios

	sun tracking	2 degree/s rotation	4 degree/s rotation	6 degree/s rotation
Mean absolute error of T estimation	1.5780°C	2.1690°C	2.1961°C	2.5513°C
Mean absolute error of G estimation	2.9027W/m^2	1.8924W/m^2	2.1000W/m^2	2.9027W/m^2
Mean absolute error of V_{mp} estimation	0.2054V	0.2564V	0.2512V	0.2770V

To compare with the SIMPPE algorithm and the conventional MPPT methods, the tracking efficiency of the TMPPE algorithm is calculated using (3.1) and illustrated in Table 5.3.

Table 5.3 Comparison of tracking efficiencies under different satellite operating scenarios

	sun tracking	2 degree/s rotation	4 degree/s rotation	6 degree/s rotation
TMPPE	96.80%	95.13 %	95.05%	94.96%
SIMPPE	99.80%	98.29 %	98.17 %	98.07 %
P&O (best case)	99.64% (ΔD = 1%)	92.28% (ΔD = 3%)	85.64% (ΔD = 4%)	93.11% (ΔD = 1%)
InC (best case)	99.64% (ΔD = 1%)	92.34% (ΔD = 3%)	85.56% (ΔD = 4%)	93.15% (ΔD = 1%)

As was expected, the TMPPE algorithm has slightly lower tracking performance compared to the SIMPPE algorithm. This is due to the fact there are some power losses associated with the acquisition process. However, the TMPPE algorithm is able to estimate the MPP without temperature sensor as compared to the SIMPPE

algorithm. Compared to the conventional MPPT methods, the TMPPE algorithm has slight improvement of 1% to 10% of tracking efficiency in satellite safe-hold operating scenarios.

5.4. **Experimental Validation of TMPPE Algorithm**

To validate the TMPPE algorithm experimentally, the hardware-in-the-loop test system in Fig. 4.17 is used. Four experiments have been conducted to validate the TMPPE algorithm in Algorithm 5.1 with four different satellite scenarios in Fig. 3.3 are used. The comparison between simulation and experimental results are presented in Fig. 5.14.

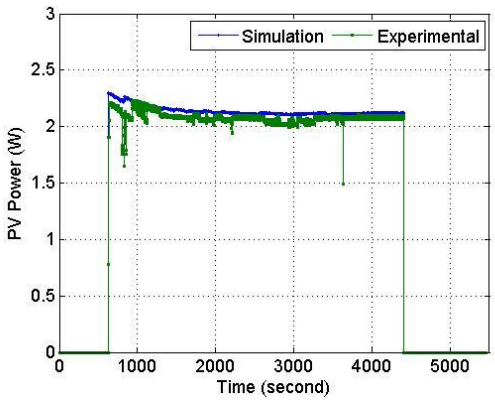

(a) Normal operating mode with sun-tracking

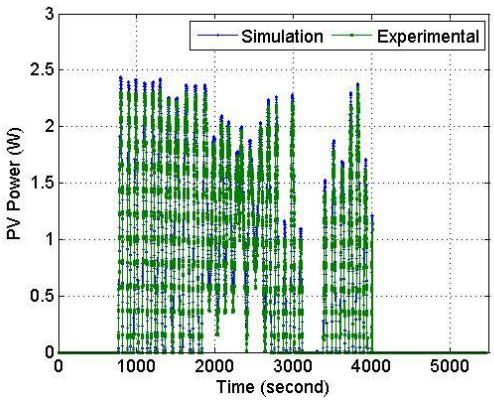

(b) Safe-hold operating mode with 2 degrees/s rotation

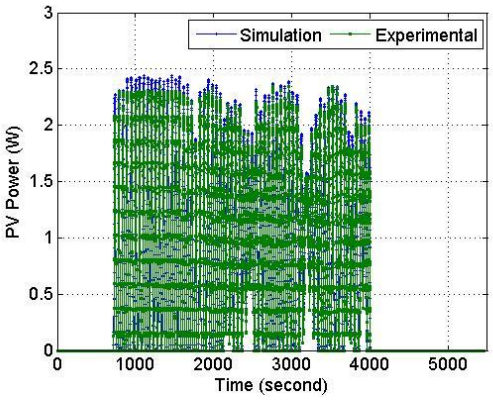

(c) Safe-hold operating mode with 4 degrees/s rotation

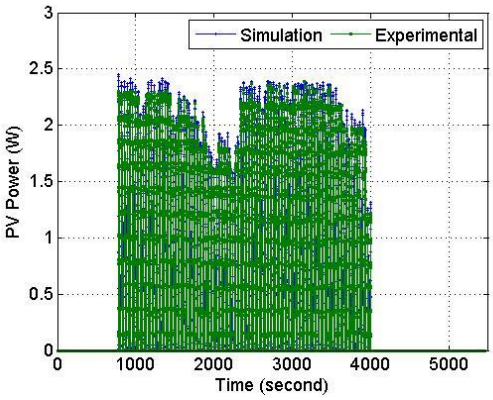

(d) Safe-hold operating mode with 6 degrees/s rotation

Fig. 5.14 Experimental tracked power vs simulation tracked power for TMPPE algorithms under different scenarios

From Fig. 5.14, it is observed that the experimental results match with the simulation results. Similar to the SIMPPE algorithm, the difference of simulation and experimental results is less than 0.2W at most of the time in all satellite operating scenarios. The tracking efficiency of both simulation and experimental are calculated and compared in Table 5.4.

Table 5.4 Tracking efficiency comparison for the TMPPE algorithm

	sun tracking	2 degree/s rotation	4 degree/s rotation	6 degree/s rotation
Simulation	96.80%	95.13 %	95.05%	94.96%
Experimental	92.94%	87.62%	87.78%	87.90%

Thus, the tracking performance of the TMPPE algorithm have been validated. Comparing Table 5.4 with Table 4.6, the TMPPE algorithm has poorer tracking efficiency when compared with SIMPPE algorithm. This is because of the four point measurements used by the TMPPE algorithm, which resulted in power losses during

acquisition process. However, the TMPPE algorithm has the advantage of removing the use of a temperature sensor as compared to the SIMPPE algorithm.

5.5. **Summary**

The feasibility of the TMPPE algorithm has been investigated under different measurement noise that range from 0.1% to 1.0% of the measurement. The simulation result shows that the TMPPE algorithm gives less than 1% V_{mp} estimation error and its tracking efficiency is above 98%. This show that the tracking performance of the proposed method is not sensitive to measurement noise. To further study the feasibility of TMPPE algorithm under different environmental conditions with temperature and solar insolation level that range from -20°C to 140°C and 200W/m^2 to 1200W/m^2, the simulation have been conducted using Monte Carlo approach. The TMPPE algorithm gives tracking efficiency of 99% at 3-sigma for 0.5% measurement noise.

The performance of the TMPPE algorithm has been further validated using PSIM-based simulation. The simulation results show that the tracking efficiency of TMPPE algorithm has improved between 1% and 10% comparing to the best case of P&O and InC in satellite safe-hold operating scenarios. Finally, the TMPPE algorithm has been validated experimentally using hardware-in-the-loop test system. The experimental results show that the tracking efficiency are 92% and 87% respectively for normal and safe-hold operating scenarios.

CHAPTER 6. CONCLUSION AND FUTURE WORKS

6.1. Conclusion

In this thesis, a PSIM-based simulation study has been conducted using the conventional MPPT methods (P&O and InC) for space application. The results show that the tracking performance of the conventional MPPT methods has above 90% tracking efficiency in normal operation scenario. However, for satellite operating in safe-hold scenarios, the tracking efficiency of P&O and InC deteriorate by 37.52% and 37.13% respectively when the satellite is rotating at 6 degree/s.

To overcome these shortcomings, a SIMPPE algorithm based on a single diode PV model has been developed. The SIMPPE algorithm estimates the solar insolation of PV using voltage, current and temperature measurement. With the estimated solar insolation, the SIMPPE algorithm is able to perform MPPT by generating *I-V* curve using Newton-Raphson method. Comparing to the conventional MPPT methods, it required an additional of temperature sensor while P&O and InC needs only voltage and current readings to perform MPPT.

The feasibility of the SIMPPE algorithm has been investigated under different temperatures (-30°C to 150°C) and solar insolation level (1W/m^2 to 1353W/m^2). The simulation results show that the SIMPPE algorithm has a low solar insolation estimation error of less than 3W/m^2 in all cases and a low V_{mp} estimation error of less than 0.05V in 95% of cases. The performance of the SIMPPE algorithm has been further validated using PSIM-based simulation. The simulation results show that the SIMPPE algorithm is able to maintain the tracking performance above 97% in all satellite scenarios. In normal operation scenario, the SIMPPE algorithm has an

improved 0.4% of tracking efficiency comparing to the best case of the conventional MPPT methods. However, in safe-hold operation scenario, the tracking efficiency of SIMPPE algorithm has improved between 0.47% and 12.36% comparing to the best case of the conventional MPPT methods for different rotation rates. Finally, experiments has conducted using a hardware-in-the-loop test system to validate the SIMPPE algorithms.

A TMPPE algorithm has been proposed to solve for PV MPP with only voltage and current measurements. The TMPPE estimates the temperature and solar insolation of PV using four pairs of PV voltage and current measurements. Similar to SIMPPE algorithm, the TMPPE estimate the MPP voltage by solving *I-V* equation using Newton-Raphson method.

The performances of the TMPPE algorithm has been validated through simulation and experiments. The feasibility of the TMPPE algorithm has been investigated in simulation under different measurement noise environment. The simulation results show that the TMPPE algorithm has achieved less than 1% power loss at 3-sigma for case when solar insolation level is above 600W/m^2. The performance of the TMPPE algorithm has been further validated using PSIM-based simulation. The simulation results show that the TMPPE has improved tracking efficiency of between 0.21% and 9.49% compared to the conventional MPPT methods. Finally, the experimental results have validated the TMPPE algorithm.

6.2. **Future Works**

The following suggestions should be explored further for the future works.

In this thesis, the performance of the SIMPPE algorithm and the TMPPE algorithm is limited by single diode PV model. It deteriorates when the PV operating points is approaching open circuit voltage at low solar insolation level. The PV modelling accuracy can be improved further using double diode PV model [49, 50]. For future research, the MPP estimation algorithm based on double diode PV model can be considered.

Besides that, it was identified that the temperature and solar insolation level estimation of TMPPE algorithm is affected by the measurement noise. Thus, developing a filtering algorithm to the measurement noise is an advantage. The PV environmental condition estimation can be achieved by implementing a Kalman filter to reduce measurement noise to have better estimation accuracy.

In this research, the solar insolation level and temperature estimation algorithm is developed based on four measurement points. It is known that P&O and InC methods have steady-state oscillation issue. Thus, the estimation algorithm can be integrated with the P&O and InC methods to estimate the temperature and solar insolation level while performing the MPPT.

LIST OF PUBLICATIONS

[1] **J. M. Lew**, K. S. Low, H. Aung, and J. J. Soon, "In-Orbit Performance of VELOX-PII Power Management System," in *Proc. Int. Symp. on Space Technology and Sci., JSASS*, Kobe, Japan, Jul. 2015.

[2] L. S. Lim, T. D. V. Bui, Z. Lau, M. S. C. Tissera, J. J. Soon, **J. M. Lew**, H. Aung, C. Ye, K. S. Low, S. T. Goh, and S. S. Chen, "Development and design challenges in VELOX-I nanosatellite," in *Proc. Int. Conf. Space Sci. and Commun. (IconSpace)*, Langkawi, Malaysia, Aug. 2015.

[3] **J. M. Lew**, H. Aung, J. J. Soon, and K. S. Low, "In-Flight Data Studies of VELOX-II Power Management System," in *Small Satellites, Syst. & Services Symp. (4S)*, Valletta, Malta, May. 2016.

[4] J. J. Soon, K. S. Low, H. Aung, and **J. M. Lew**, "In-Orbit Performance of Singapore's First Indigenous Micro-Satellite – X-SAT," in *Small Satellites, Syst. & Services Symp. (4S)*, Valletta, Malta, May. 2016.

[5] **J. M. Lew**, H. Aung, J. J. Soon, and K. S. Low, "Evaluating the In-Orbit Performance of Power Management System for the VELOX-PII Satellite," *Trans. of the Japan Soc. for Aeronautical and Space Sci. Aerospace Technology Japan*, vol. 14, no.ists30, pp. Pf_69-Pf_75, Sep. 2016.

[6] L. S. Lim, T. D. V. Bui, M. S. C. Tissera, V. H. P. Pham, R. Abhishek, J. J. Soon, **J. M. Lew**, H. Aung, K. S. Low, S. T. Goh, and S. S. Chen, "VELOX-II: Challenges of developing a 6U nanosatellite," in *AIAA Space and Astronautics Forum and Exposition*, Long Beach, California, Sep. 2016.

[7] S. T. Goh, L. S. Lim, T. D. V. Bui, M. S. C. Tissera, V. H. P. Pham, R. Abhishek, J. J. Soon, **J. M. Lew**, H. Aung, G. X. Lee, J. W. Chia, K. W. Chow, S. Ankit, L. Deng, and K. S. Low, "VELOX-II: Summary of one year in operation," (submitted to *Int. Symp. on Space Technology and Sci., JSASS,* Matsuyama-Ehime, Japan, Jun. 2017)

[8] J. J. Soon, J. W. Chia, H. Aung, **J. M. Lew**, S. T. Goh, and K. S. Low, "A Photovoltaic-Model-Based-Method to Monitor Solar-Array Degradation On-Board a Micro-Satellite," (submitted to *IEEE Transaction on Aerospace and Electronic Systems*)

BIBLIOGRAPHY

[1] H. Heidt, J. Puig-Suari, A. Moore, S. Nakasuka, and R. Twiggs, "CubeSat: A new generation of picosatellite for education and industry low-cost space experimentation," 2000.

[2] K. Woellert, P. Ehrenfreund, A. J. Ricco, and H. Hertzfeld, "Cubesats: Cost-effective science and technology platforms for emerging and developing nations," *Advances in Space Research*, vol. 47, no. 4, pp. 663-684, Feb. 2011.

[3] J. Bouwmeester and J. Guo, "Survey of worldwide pico- and nanosatellite missions, distributions and subsystem technology," *Acta Astronautica*, vol. 67, no. 7–8, pp. 854-862, Oct. 2010.

[4] D. Selva and D. Krejci, "A survey and assessment of the capabilities of Cubesats for Earth observation," *Acta Astronautica*, vol. 74, no. 0, pp. 50-68, May. 2012.

[5] S. Nakasuka, N. Sako, H. Sahara, Y. Nakamura, T. Eishima, and M. Komatsu, "Evolution from education to practical use in University of Tokyo's nano-satellite activities," *Acta Astronautica*, vol. 66, no. 7–8, pp. 1099-1105, Apr. 2010.

[6] F. Santoni, F. Piergentili, S. Donati, M. Perelli, A. Negri, and M. Marino, "An innovative deployable solar panel system for Cubesats," *Acta Astronautica*, vol. 95, pp. 210-217, Feb. 2014.

[7] A. Ali, M. R. Mughal, H. Ali, and L. Reyneri, "Innovative power management, attitude determination and control tile for CubeSat standard NanoSatellites," *Acta Astronautica*, vol. 96, pp. 116-127, Mar. 2014.

[8] M. F. Rose, "Space power technology," in *Proc. 22nd Int. Power Modulator Symp.*, Boca Raton, FL, Jun. 1996, pp. 9-14.

[9] G. L. Bennett and E. A. Skrabek, "Power performance of US space radioisotope thermoelectric generators," in *Proc. 15th Int. Conf. Thermoelectrics*, Pasadena, CA, USA, Mar. 1996, pp. 357-372.

[10] J. C. Bass and D. T. Allen, "Milliwatt radioisotope power supply for space applications," in *Thermoelectrics, 1999. Eighteenth International Conference on*, Sep. 1999, pp. 521-524.

[11] L. Cristaldi, M. Faifer, M. Rossi, and S. Toscani, "MPPT definition and validation: A new model-based approach," in *Proc. IEEE Int. Instrumentation and Measurement Technology Conf. (I2MTC)*, Graz, May. 2012, pp. 594-599.

[12] T. Esram and P. L. Chapman, "Comparison of Photovoltaic Array Maximum Power Point Tracking Techniques," *IEEE Trans. Energy Convers.*, vol. 22, no. 2, pp. 439-449, Jun. 2007.

[13] B. Bendib, H. Belmili, and F. Krim, "A survey of the most used MPPT methods: Conventional and advanced algoithms applied for photovolatic systems," *Renew Sustain Energy*, no. 45, pp. 637-648, May. 2015.

[14] H. Rezk and A. M. Eltamaly, "A comprehensive comparison of different MPPT techniques for photovoltaic systems," *Solar Energy*, vol. 112, pp. 1-11, Feb. 2015.

[15] B. Subudhi and R. Pradhan, "A Comparative Study on Maximum Power Point Tracking Techniques for Photovoltaic Power Systems," *IEEE Trans. Sustain. Energy*, vol. 4, no. 1, pp. 89-98, Jan. 2013.

[16] M. A. Elgendy, B. Zahawi, and D. J. Atkinson, "Assessment of Perturb and Observe MPPT Algorithm Implementation Techniques for PV Pumping Applications," *IEEE Trans. Sustain. Energy*, vol. 3, no. 1, pp. 21-33, Jan. 2012.

[17] A. K. Abdelsalam, A. M. Massoud, S. Ahmed, and P. Enjeti, "High-Performance Adaptive Perturb and Observe MPPT Technique for Photovoltaic-Based Microgrids," *IEEE Trans. Power Electron.*, vol. 26, no. 4, pp. 1010-1021, Apr. 2011.

[18] A. Pandey, N. Dasgupta, and A. K. Mukerjee, "High-Performance Algorithms for Drift Avoidance and Fast Tracking in Solar MPPT System," *IEEE Trans. Energy Convers.*, vol. 23, no. 2, pp. 681-689, Jun. 2008.

[19] N. Fermia, D. Granozio, G. Petrone, and M. Vitelli, "Predictive & Adaptive MPPT Perturb and Observe Method," *IEEE Trans. Aerosp. Electron. Syst.*, vol. 43, no. 3, pp. 934-950, Jul. 2007.

[20] M. A. G. de Brito, L. Galotto, L. P. Sampaio, G. de Azevedo e Melo, and C. A. Canesin, "Evaluation of the Main MPPT Techniques for Photovoltaic Applications," *IEEE Trans. Ind. Electron.*, vol. 60, no. 3, pp. 1156-1167, Mar. 2013.

[21] P.-C. Chen, P.-Y. Chen, Y.-H. Liu, J.-H. Chen, and Y.-F. Luo, "A comparative study on maximum power point tracking techniques for photovoltaic generation systems operating under fast changing environments," *Solar Energy*, vol. 119, pp. 261-276, Sep. 2015.

[22] A. A. Elbaset, H. Ali, M. A.-E. Sattar, and M. Khaled, "Implementation of a modified perturb and observe maximum power point tracking algorithm for photovoltaic system using an embedded microcontroller," *IET Renewable Power Gen.*, vol. 10, no. 4, pp. 551-560, Apr. 2016.

[23] M. Killi and S. Samanta, "Modified Perturb and Observe MPPT Algorithm for Drift Avoidance in Photovoltaic Systems," *IEEE Transactions on Industrial Electronics*, vol. 62, no. 9, pp. 5549-5559, Feb. 2015.

[24] A. Safari and S. Mekhilef, "Simulation and Hardware Implementation of Incremental Conductance MPPT With Direct Control Method Using Cuk Converter," *IEEE Trans. Ind. Electron.*, vol. 58, no. 4, pp. 1154-1161, Apr. 2011.

[25] M. A. Elgendy, B. Zahawi, and D. J. Atkinson, "Assessment of the Incremental Conductance Maximum Power Point Tracking Algorithm," *IEEE Trans. Sustain. Energy*, vol. 4, no. 1, pp. 108-117, Jan. 2013.

[26] L. Fangrui, D. Shanxu, L. Fei, L. Bangyin, and K. Yong, "A Variable Step Size INC MPPT Method for PV Systems," *IEEE Trans. Ind. Electron.*, vol. 55, no. 7, pp. 2622-2628, Jul. 2008.

[27] H. Guan-Chyun, I. H. Hung, T. Cheng-Yuan, and W. Chi-Hao, "Photovoltaic Power-Increment-Aided Incremental-Conductance MPPT With Two-Phased Tracking," *IEEE Trans. Power Electron.*, vol. 28, no. 6, pp. 2895-2911, Jun. 2013.

[28] K. H. Hussein, I. Muta, T. Hoshino, and M. Osakada, "Maximum photovoltaic power tracking: an algorithm for rapidly changing atmospheric conditions," *IEE Proc. Generation, Transmission and Distribution*, vol. 142, no. 1, pp. 59-64, Jan. 1995.

[29] M. A. S. Masoum, H. Dehbonei, and E. F. Fuchs, "Theoretical and experimental analyses of photovoltaic systems with voltage and current-based maximum power-point tracking," *IEEE Trans. Energy Convers.*, vol. 17, no. 4, pp. 514-522, Dec. 2002.

[30] J. Ahmad, "A fractional open circuit voltage based maximum power point tracker for photovoltaic arrays," in *Proc. 2nd Int. Conf. Software Technology and Engineering (ICSTE)*, San Juan, PR, Oct. 2010, pp. V1-247-V1-250.

[31] Y. P. Huang, "A Rapid Maximum Power Measurement System for High-Concentration Photovoltaic Modules Using the Fractional Open-Circuit Voltage Technique and Controllable Electronic Load," *IEEE J. Photovoltaics*, vol. 4, no. 6, pp. 1610-1617, Nov. 2014.

[32] A. Sandali, T. Oukhoya, and A. Cheriti, "Modeling and design of PV grid connected system using a modified fractional short-circuit current MPPT," in *Proc. Int. Renewable and Sustainable Energy Conference (IRSEC)*, Oct. 2014, pp. 224-229.

[33] M. Veerachary, T. Senjyu, and K. Uezato, "Neural-network-based maximum-power-point tracking of coupled-inductor interleaved-boost-converter-supplied PV system using fuzzy controller," *IEEE Trans. Ind. Electron.*, vol. 50, no. 4, pp. 749-758, Aug. 2003.

[34] T. L. Kottas, Y. S. Boutalis, and A. D. Karlis, "New maximum power point tracker for PV arrays using fuzzy controller in close cooperation with fuzzy cognitive networks," *IEEE Trans. Energy Convers.*, vol. 21, no. 3, pp. 793-803, Sep. 2006.

[35] Craig S. Clark and A. L. Mazarias, "Power system challenges for small satellite missions," in *Proc. Small Satellites, Systems and Services Symp.*, Chia Laguna, Sardinia, Italy, Sep. 2006.

[36] M. C. Mahdi, J. S. Jaafer, and A.-A.-R. Shehab, "Design and Implementation of an Effective Electrical Power System for Nano-Satellite," *International Journal of Scientific & Engineering Research*, vol. 5, no. 5, May, 2014.

[37] M. Pajusalu, E. Ilbis, T. Ilves, M. Veske, J. Kalde, H. Lillmaa, *et al.*, "Design and pre-flight testing of the electrical power system for the ESTCube-1 nanosatellite," *Proceedings of the Estonian Academy of Sciences*, vol. 63, no. 2s, pp. 232-241, Jun, 2014.

[38] J. J. Soon and K. S. Low, "Photovoltaic Model Identification Using Particle Swarm Optimization With Inverse Barrier Constraint," *IEEE Trans. Power Electron.*, vol. 27, no. 9, pp. 3975-3983, Sep. 2012.

[39] M. G. Villalva, J. R. Gazoli, and E. R. Filho, "Comprehensive Approach to Modeling and Simulation of Photovoltaic Arrays," *IEEE Trans. Power Electron.*, vol. 24, no. 5, pp. 1198-1208, May. 2009.

[40] D. Sera, R. Teodorescu, and P. Rodriguez, "PV panel model based on datasheet values," in *Proc. IEEE Int. Symp. Ind. Electron. (ISIE)*, Vigo, Spain, Jun. 2007, pp. 2392-2396.

[41] K. Yeong-Chan, L. Tsorng-Juu, and C. Jiann-Fuh, "Novel maximum-power-point-tracking controller for photovoltaic energy conversion system," *IEEE Trans. Ind. Electron.*, vol. 48, no. 3, pp. 594-601, Jun. 2001.

[42] S. Liu and R. A. Dougal, "Dynamic multiphysics model for solar array," *IEEE Trans. Energy Convers.*, vol. 17, no. 2, pp. 285-294, Jun. 2002.

[43] D. Y. Lee, J. W. Cutler, J. Mancewicz, and A. J. Ridley, "Maximizing photovoltaic power generation of a space-dart configured satellite," *Acta Astronautica*, vol. 111, pp. 283-299, Jun. 2015.

[44] D. Sera, L. Mathe, T. Kerekes, S. V. Spataru, and R. Teodorescu, "On the Perturb-and-Observe and Incremental Conductance MPPT Methods for PV Systems," *IEEE J. Photovoltaics*, vol. 3, no. 3, pp. 1070-1078, Jul. 2013.

[45] J. M. Lew, H. Aung, J. Jun Soon, and K. S. Low, "Evaluating the In-Orbit Performance of Power Management System for the VELOX-PII Satellite," *Trans. of the Japan Soc. for Aeronautical and Space Sci. Aerospace Technology Japan*, vol. 14, no. ists30, pp. Pf_69-Pf_75, Sep. 2016.

[46] L. Cristaldi, M. Faifer, M. Rossi, and S. Toscani, "An Improved Model-Based Maximum Power Point Tracker for Photovoltaic Panels," *IEEE Trans. Instrum. Meas.*, vol. 63, no. 1, pp. 63-71, Jan. 2014.

[47] J. M. Blanes, F. J. Toledo, S. Montero, and A. Garrig, "In-Site Real-Time Photovoltaic I-V Curves and Maximum Power Point Estimator," *IEEE Trans. Power Electron.*, vol. 28, no. 3, pp. 1234-1240, Mar. 2013.

[48] C. Carrero, J. Amador, and S. Arnaltes, "A single procedure for helping PV designers to select silicon PV modules and evaluate the loss resistances," *Renewable Energy*, vol. 32, no. 15, pp. 2579-2589, Dec. 2007.

[49] K. Ishaque, Z. Salam, and H. Taheri, "Simple, fast and accurate two-diode model for photovoltaic modules," *Solar Energy Materials and Solar Cells*, vol. 95, no. 2, pp. 586-594, Feb. 2011.

[50] N. M. A. A. Shannan, N. Z. Yahaya, and B. Singh, "Single-diode model and two-diode model of PV modules: A comparison," in *Proc. IEEE Int. Conf. Control Syst., Computing and Eng. (ICCSCE)*, Penang, Malaysia, Nov. 2013, pp. 210-214.